UNIVERSITEIT VAN PRETORIA
UNIVERSITY OF PRETORIA
YUNIBESITHI YA PRETORIA

A FEASIBILITY STUDY ON THE USE OF MAGNETIC INDUCTANCE TO CHARGE WIRELESS SENSOR NODES

By

Nicolaas Aling Vorster

Studyleader: Prof. GP Hancke

Submitted in partial fulfillment of the requirements for the degree

Master of Engineering (Electronics)

in the

Department of Electrical, Electronic & Computer Engineering

in the

School of Engineering

in the

Faculty of Engineering, Built Environment & Information Technology

UNIVERSITY OF PRETORIA

May 2010

© University of Pretoria

SUMMARY

A FEASIBILITY STUDY ON THE USE OF MAGNETIC INDUCTANCE TO CHARGE WIRELESS SENSOR NODES

by

Nicolaas Aling Vorster

Studyleader: Prof. GP Hancke

Department of Electrical, Electronic & Computer Engineering

Master of Engineering (Electronics)

A Wireless Sensor Network (WSN) is a group of sensors which are used to monitor or detect phenomena. These sensors are capable of transferring sensed data wirelessly.

Power supply is a key issue in a WSN. The lifetime of the WSN node's batteries is limited, thereby limiting the effective lifetime of the node. There is need for ways to recharge batteries wirelessly. Magnetic inductive power transfer might provide an alternative way of recharging WSN nodes, rather than with energy scavenging techniques.

This research investigates the use of magnetic inductive power transfer techniques in WSNs. A system used to recharge a WSN node is limited in terms of minimum efficiency, size, and separation distance between the coils.

In order to maximise efficiency for small coil sizes, this research focuses on resonant, mid-range power transfer in the near-field region. A new coil type, the hybrid coil, is proposed and the theory to calculate its parameters is presented. A total of four coil types are investigated and compared with each other theoretically and experimentally.

The effects of various parameter tolerances are investigated, including the effect of non-resonant operation, the effect of increasing the primary coil size and the effect of misaligned coil centres.

The results show that magnetic inductive power transfer is not yet efficient enough to make it a viable option for use in WSNs. In addition, the results show that the hybrid coil proposed in this dissertation outperforms any of the other coil types.

Keywords:

Coupling coefficient

Energy efficient

Hybrid coils

Magnetic inductive power transfer

Medium distance power transfer

Power transfer efficiency

Resonant coupling

Wireless power transfer

Wireless Sensor Network node power supply

Wireless Sensor Networks.

OPSOMMING

A FEASIBILITY STUDY ON THE USE OF MAGNETIC INDUCTANCE TO CHARGE WIRELESS SENSOR NODES

deur

Nicolaas Aling Vorster

Studieleier: Prof. GP Hancke

Departement Elektriese-,Elektroniese- & Rekenaar Ingenieurswese

Meester in Ingenieurswese (Elektronies)

’n Draadlose Sensornetwerk (DSN) is ’n groep sensors wat gebruik word om verskynsels te monitor en op te spoor. Hierdie sensors is in staat daartoe om waargenome data sonder enige fisiese verbinding oor te dra.

Kragtoevoer is ’n kern vraagstuk in ’n DSNe. Die leeftyd van ’n DSN nodus se battery is beperk en beperk dus die effektiewe leeftyd van die DSN nodus self. Daar is ’n behoefte vir maniere om die batterye draadloos te herlaai. Magneties induktiewe kragoorplasing kan moontlik ’n alternatiewe manier wees om DSN nodusse te herlaai, eerder as met energie opgaar tegnieke.

Hierdie navorsing ondersoek die gebruik van magneties induktiewe kragoorplasing in DSNe. ’n Stelsel wat gebruik word om ’n DSN nodus te herlaai is beperk in terme van minimum effektiwiteit, grootte en die afstand tussen die spoele.

Om die effektiwiteit van klein spoele te maksimeer fokus hierdie navorsing op resonante, medium afstand, kragoorplasing in die naby-veld omgewing. ’n Nuwe tipe spoel, die saamgestelde spoel, word voorgestel en die teorie om die spoel se parameters te bepaal word gegee. ’n Totaal van vier spoel tipes word ondersoek en teoreties en eksperimenteel met mekaar vergelyk.

Die invloed van verskeie parameter toleransies word ondersoek, insluitende die gevolg van nie-resonante werking, die effek van ’n vergroting van die primêre spoel en die effek van spoel middelpunte wat nie in lyn met mekaar is nie.

Die resultate wys dat magneties induktiewe kragoorplasing nog nie effektief genoeg is om ’n praktiese opsie vir DSNe te wees nie. Verder wys die resultate ook dat die saamgestelde spoel wat in hierdie verhandeling voorgestel word beter resultate lewer as enige van die ander tipes spoele.

Sleutelwoorde:
Draadlose kragoorplasing
Draadlose Sensornetwerk kragtoevoer
Draadlose Sensornetwerke
Energie effektief
Koppelings koeffisiënt
Kragoorplasings effektiwiteit
Magneties induktiewe kragoorplasing
Medium afstand kragoorplasing
Resonante koppeling
Saamgestelde spoele.

To my loving family

who supported me through my years of study

and

to God Almighty for giving me talents,

and the opportunities to use them.

ACKNOWLEDGEMENTS

ABBREVIATIONS

DC	Direct Current
ICNIRP	International Commission on Non-Ionizing Radiation Protection
MEMS	Microelectromechanical
OFET	Organic Field Effect Transistor
PDA	Personal Digital Assistant
SAR	Specific Absorption Rate
SRAM	Static Random Access Memory
TET	Transcutaneous Energy Transformer
WSN	Wireless Sensor Network

CONTENTS

LIST OF FIGURES

LIST OF TABLES

CHAPTER ONE

RESEARCH OVERVIEW

"One possibility for providing an implanted stimulator transcutaneously with power and/or information is to transmit RF power via an inductive link."

C.M. Ziefhofer and E.S. Hochmair [1] - 1990

"We were able to transfer 60 watts with ∼40% efficiency over distances in excess of 2 meters."

A. Kurs et al [2] - 2007

1.1 INTRODUCTION

THIS dissertation will investigate the feasibility of using magnetic inductive techniques to charge wireless sensor nodes.

WSNs (Wireless Sensor Networks) are limited by power supply. Unless externally powered, a sensor is dependent on its batteries' lifetime. While increased battery capacity does increase the sensor's lifetime, it also increases cost and size. Various energy scavenging techniques to recharge sensor batteries have been investigated, ranging from converting seismic vibrations [3] or thermal gradients [4] to energy, to converting ambient radio signals to energy [5]. While these techniques have great potential, Körber *et al* [6] has shown that it is not yet possible to source enough power from only one of these sources. Some solutions, such as piezoelectric materials, can provide adequate power to use a radio transmitter, but only at very low duty cycles [7].

If feasible, magnetic inductive techniques will be an alternative means to recharge WSN nodes in situations where energy scavenging techniques cannot provide adequate power to

operate the WSN nodes or where the required duty cycle of the WSN nodes is too high to be accommodated by energy scavenging techniques.

Current research in magnetic inductive power transfer is focused on short range power transfer, where the diameter of the transmitting coil is larger than distance of power transfer. Obviously this will not be acceptable for the case of a WSN where the distance between the transmitter and the receiver is in the meter range. Despite the advantages of using magnetic inductive techniques it is not yet clear whether it is indeed possible to design an inductive link that is both efficient enough and small enough to be used in a WSN.

This dissertation will provide a discussion on current coil types and models, and on the current applications for magnetic inductive power transfer.

1.2 SCOPE

This dissertation is focused on determining whether magnetic inductive power transfer is a feasible solution to charge wireless sensor nodes, and to design and model an inductive coil to use as both a power transmitter and as a power receiver.

1.3 PROBLEM STATEMENT

Whenever research is done on WSNs, one of the most important considerations is power efficiency. Power efficiency influences the lifetime of the sensor, the required battery size, and ultimately the cost of the sensor. There is a great need for a way to charge wireless sensor nodes in a way that is efficient and inexpensive.

Present recharging methods [8] include, but are not limited to:

- solar power,
- hydro generation,
- environmental vibration harvesting
- and wind flow generation.

Above mentioned methods, however, are dependent on environmental conditions. They are primarily applicable in outdoor environments. Options that might be of use indoors are solar power, and then only if the sensor is placed near a window, and environmental vibration

harvesting which can be used in environments with high levels of vibration. For an indoor environment with low vibration levels, a different method is necessary.

Another factor that must be taken into account is the cost of the WSN node. In a system where the number of WSN nodes are large, expensive recharging techniques will result in a large increase in the total cost of the system. The maintenance of the system must also be taken into account. An all-electrical system that uses a copper coil to recharge the WSN nodes will be less expensive and easier to maintain than a system that contains mechanical parts such as generators.

The basic parameters of a magnetic inductive system used to recharge WSN nodes that must be taken into account are:

- the power transfer efficiency,
- the operating distance,
- the maximum size of the transmitter and the receiver coils,
- and the maximum power output allowed for the transmitter coil.

These parameters will be discussed in more detail in Chapter 4.

1.4 RESEARCH APPROACH

The approach followed in this dissertation focuses on whether magnetic inductance is a feasible option. Although the field of magnetic inductive power transfer is an old one that is used extensively in transformers, this application has inherent difficulties that need to be investigated. While a standard transformer use some kind of core to transfer the magnetic flux, a magnetic inductive system for use in WSNs will have an air core, which decreases the power transfer efficiency. In a WSN the distance between the two coils is much greater than in a transformer, and the limitation on the device size is an even greater concern than it already is for transformers.

1.4.1 Hypothesis Formulation

The hypothesis that was formulated for this dissertation is:

Magnetic inductive techniques can be used to recharge WSN nodes over a medium sized office by using inductive coils that are effective in terms of power transfer efficiency, cost and size comparable to a WSN node.

The detailed specifications to evaluate a magnetic inductive power transfer system are given in Section 4.4.

1.4.2 Research Questions

Some of the issues to be discussed in this dissertation include:

- How do solenoid type coils and planar coils compare with respect to power transfer efficiency?
- What mathematical models can be used for both solenoid type coils and for planar type coils to determine their power transfer efficiency?
- A coil must be designed that has high power transfer efficiency, low cost and small size.
- A mathematical model for the designed coil must be created, and the power transfer efficiency when using that coil must be determined.
- Over what distance can a WSN node be recharged using magnetic inductive techniques?
- Is magnetic inductive techniques suitable to recharge WSNs?

By answering these questions, the feasibility of magnetic inductive techniques for the recharge of WSN nodes will be determined.

1.5 DOCUMENT OUTLAY

The dissertation has the following outlay:

- **Chapter 1** is an overview of the research that will be done in this dissertation.
- **Chapter 2** is a literature study. In this Chapter the current literature on existing applications for magnetic inductive power transfer techniques and on various coil types is discussed.

- **Chapter 3** gives a quick overview of the different coil types that are found in wireless power transfer systems.
- **Chapter 4** describes the basic setup of a magnetic inductive power transfer system and states operational requirements of the system.
- **Chapter 5** explains the principal of mid-range power transfer in the near-field region, and applies its theory to the various coil types.
- **Chapter 6** compares the different coil types to each other mathematically.
- **Chapter 7** discusses a practical inductive power transfer system used to investigate the various coil types.
- **Chapter 8** explains the effects of various device tolerances on the efficiency and coupling coefficient of an inductive power transfer system.
- **Chapter 9** concludes this dissertation and proposes future work in this field.

1.6 CHAPTER SUMMARY

In this Chapter the problem to be addressed in this dissertation is introduced and stated. The scope of the dissertation and the research approach to be used is given. The research questions to be answered in this dissertation are given, and a formal hypotheses is stated. Finally, an outlay of the dissertation is given.

CHAPTER TWO
LITERATURE STUDY

"If we knew what it was we were doing, it would not be called research, would it?"

Attributed to A. Einstein

MUCH of the available literature on the use of magnetic inductive techniques for power transfer focus on very short range applications [1] [9] [10]. Very little mention is made of power transfer over longer distances [2].

The bulk of the available literature focus on the use of magnetic inductive techniques in transcutaneous links [11], which was one of the first applications for magnetic inductive links outside the traditional use in transformers.

The following parts will discuss the current applications and feasibility of magnetic inductive techniques for power transfer and the mathematical models available for the two most prominent coil types: planar coils and solenoid coils.

2.1 GENERAL FEASIBILITY

Inductive links for medical applications has been researched in much detail. In 1961 already, a transcutaneous energy transformer (TET) [11] was developed to power artificial hearts. It uses planar coils which are coupled in the kilohertz range. The TET has a theoretical efficiency of 95% at a centimeter range. The TET's efficiency was not determined experimentally. The TET has shown that an inductive link is a feasible option for wireless power transfer.

2.2 MEDICAL LINKS

The first inductive link used for a medical application was the TET developed by Schuder *et al* in [11]. They were followed by Zierhofer and Hochmair [1] who developed methods to make the link less sensitive to misalignment [1] and to enhance the coupling coefficient of a planar coil with a geometric approach [12].

Their method to make the link less sensitive to misalignment uses feedback to vary the oscillation frequency according to the coil coupling. The oscillation frequency thus tracks the transmission efficiency maximum, whose spectral location depends on the coil coupling [1]. According to Zierfhofer and Hochmair their system is almost coupling independent up to a coil distance of 8mm, achieving an efficiency of 60% to 70%. The system uses a class E power amplifier stage, which is self oscillating. This means that additional power losses in an oscillator is avoided.

The method to enhance the coupling coefficient of a planar coil with a geometric approach shows that the coupling coefficient of the coils can be enhanced by distributing the turns of the coil across the diameter of the coil [12]. The coupling coefficient between two coils is given by

$$k_0 = \frac{M_0}{\sqrt{L_1 \cdot L_2}} \tag{2.1}$$

where k_0 is the coupling coefficient, M_0 is the mutual inductance between the two coils, and L_1 and L_2 are the self-inductances of the coils. In the case of identical transmitting and receiving coils, this simplifies to:

$$k_0 = \frac{M_0}{L_0} \tag{2.2}$$

meaning that k_0 can be increased if M_0 can be increased by a larger factor than L_0. If the radius of one of the inner turns in a planar coil is reduced, this will decrease both M_0 and L_0. The effect on L_0 will, however, be greater than the effect on M_0, which means that k_0 will increase.

The coils used by Zierhofer and Hochmair [12] had a maximum radius of 12mm and a wire radius of 0.125mm.

2.3 ELECTRIC VEHICLES

In 1999 Sakamoto *et al* [13] developed an inductive charger for electric vehicles. In the case of electric vehicles, it is possible to make the primary coil much larger than for medical applications. By using a primary coil with a radius of 0.5m they achieved 97% efficiency at a

5mm gap size. The system is capable of delivering 8.3kW output power. While these values are not applicable for WSNs, the work done by Sakamoto *et al* shows the influence of the primary coil size in the system efficiency.

In 2006 Matsuda *et al* developed a system [14] that utilizes the steel floor of the electric vehicle to assist the passing of the flux from the primary coil to the secondary coil. Their system's efficiency is 90% at a separation distance of 10cm. The system topology used is an inverter, a coupler transformer and a rectifier bridge. Matsuda *et al* also investigates the effect of the vehicle's steel floor on the system. They found that it assist in passing the magnetic flux, thereby increasing the coupling coefficient between the coils.

Matsuda *et al* [14] used a square Mn-Zn ferrite primary core of 1mx1m with a height of 10mm. Their application, which is to transfer energy for an electric vehicle, allowed them to use the vehicle's steel floor as a flux keeper, thereby increasing the efficiency of their system.

2.4 LINKS FOR MICROELECTROMECHANICAL (MEMS) SYSTEMS

Wu *et al* [15] developed an equivalent circuit for inductive links with integrated receiving coils. Their link is capable of predicting the link efficiency of the system and takes the primary coils' resistances, inductances and the secondary coil's stray capacitance into account.

Neagu *et al* [16] developed equations to characterize an electroplated planar spiral coil. The coils discussed in this article are rectangular rather than round, because rectangular coils are easier to fabricate using micromachining techniques. Equations are given to determine the self-inductance, series resistance and the parasitic capacitance of a planar spiral coil.

The coils used by Neagu *et al* had radii of 4.5μm and a wire thickness of 11μm and 1μm, respectively.

2.5 LONG DISTANCE POWER TRANSFER

A study done by Kurs *et al* [2] achieved a link efficiency of about 40% at a separation distance of more than 2m by operating in the strongly coupled region. The primary coil had a radius of 0.3m, meaning that the power transfer took place across a distance more than 6 times that of the radius of the coil.

The work done by Kurs *et al* was continued by Karalis *et al* [17]. Karalis *et al* used resonantly coupled coils in the strongly coupled domain to transfer power. Resonant coupling is a well known phenomenon in electromagnetism which is often used in coupled line filters, microwave power dividers and in microwave couplers. "'Strong coupling"' is less known in electromagnetic applications, but it is well known in light-matter interactions such as quantum optics and quantum information science [18]. According to Karalis *et al* the requirements for operations in the strongly coupled region are high Q values in order to keep the intrinsic loss rates, Γ, low, and a fast coupling rate, κ, at distances larger than the characteristic sizes of the coils.

2.6 RECYCLING OF AMBIENT MICROWAVE ENERGY

The recycling of ambient microwave energy was studied by Hagerty *et al* [19]. They used broad-band rectenna arrays. Each rectenna consists of a diode rectifier and a broad-band antenna. The greatest problem experienced with broad-band rectennas is the impedance matching between the diode rectifier and the antenna. Because both the antenna and the diode rectifier have frequency-dependant impedances, impedance matching is a challenge in a broad-band environment. Hagerty *et al* propose a frequency-independent equiangular spiral antenna to present a constant impedance to the diode rectifier. The antenna allows for dual polarization and provides convenient feed points for both the diode and the DC lines. Using these methods, Hagerty *et al* obtained power densities of 100μW to 1mW. That is comparable with the energy scavenging techniques investigated by Körber *et al* [6].

2.7 MULTI-OBJECT WIRELESS POWER TRANSMISSION SHEET

Sekitane *et al* developed a wireless power transmission sheet. The sheet comprises multiple copper transmitter coils printed on a plastic sheet. Two additional sheets respectively senses the proximity of receiver coil, and switches power to the appropriate transmitter coils. Takamiya *et al* [20] developed techniques to enhance the system proposed by Sekitane *et al*. Takamiya *et al* uses a receive coil that is double the size of the transmitter coils. They then activate several transmitter coils in the region of the receiver coil. This technique decreases the power losses if the receiver coil is not perfectly aligned with the transmitter coils. Takamiya *et al* use a line selections system that uses OFET SRAMS [21]. This approach decreases the number of

TABLE 2.1: A comparison of various magnetic inductive power transfer techniques

Type	η	D	Size	Power transfer	Cost	Ref
Transcutaneous	65%	mm	small	not given	inexpensive	[1]
Electric Vehicle Charging	90%	cm	large	2kW	more expensive	[14]
Microelectromechanical	85%	mm	small	8.1 W	micro assembly	[15]
Long Distance	40%	cm	small	60W	inexpensive	[2]

connections with off-sheet wires.

2.8 CHAPTER SUMMARY

The current literature on the subject of magnetic inductive power transfer is discussed in this Chapter. In order to make comparison of the magnetic inductive techniques discussed in this Chapter easier, the various methods are summarized in Table 2.1. This literature shows that magnetic inductive techniques can be used to supply devices wirelessly with power. Various applications are discussed, including medical links, electric vehicles, microeletromechanical systems and long distance power transfer. Although most applications uses very small distances, research [2] has shown that it is possible to achieve acceptable efficiency over larger distances. Equations to determine the parameters of a single wire loop are given.

CHAPTER THREE
COIL TYPES

MAGNETIC inductive power transfer requires some sort of device to generate and to receive the magnetic fields that are used for power transfer. Typically, some sort of wire loop or coil is used. This chapter discusses the most common coil types, as well as a new, hybrid, coil type. The most common types of coils are:

- single loops,
- solenoidal coils,
- and planar coils.

It is possible to combine these coil types in a single system in order to have for example a hybrid coil transmitter and a single loop receiver. Such a combination is expected to have better results than a system consisting of two single loops, and worse results than a system using two hybrid coils. In order to demonstrate this, a system consisting of a solenoidal coil and a single loop is investigated.

3.1 SINGLE LOOPS

The simplest form of coil that can be used is single loops, as depicted in Figure 3.1. The single loop is physically small: its height is the wire thickness, and its interior can be utilized for devices. It would be possible to place a wireless sensor node inside the coil, as long as the wireless sensor node is adequately shielded. Single loops are simple and inexpensive to manufacture. The equations to determine the parameters of a single loop are given in Section 5.3

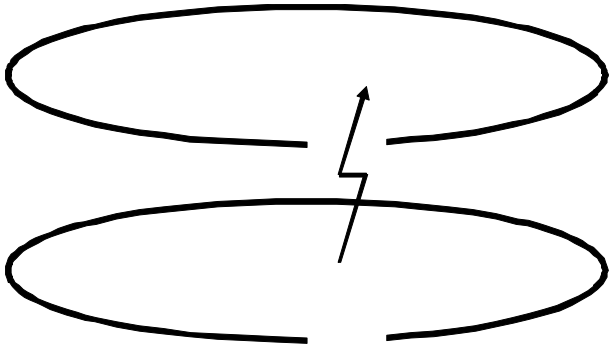

FIGURE 3.1: The single loop configuration

while the equations that applies single loops to strongly coupled, resonant power transfer are given in Section 6.1.

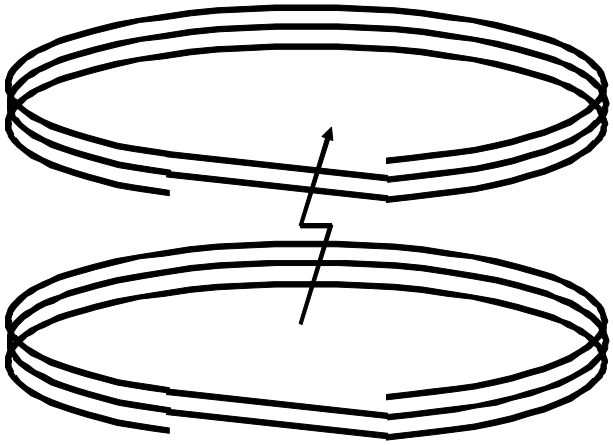

FIGURE 3.2: The solenoidal coil configuration

3.2 SOLENOIDAL COILS

The solenoidal coil, as shown in Figure 3.2, is effectively a number of single loops stacked in series on top of each other. A solenoidal coil can become quite large vertically, depending on the wire thickness, number of turns and the gap left open between turns (called the pitch). For example, a coil with $N = 10$, $pitch = 1mm$ and wire radius $a = 1mm$ will have a total thickness of $29mm$, which is a significant height in terms of wireless sensor network nodes. While simple, solenoidal coils are more difficult to manufacture than a single loop, and there is more chance of deviation from the design parameters, because of the added complexity. The coupling coefficient of a system of two solenoidal coils is higher than that of two single loops. The analytical equations for solenoidal coils are given in Section 6.2.

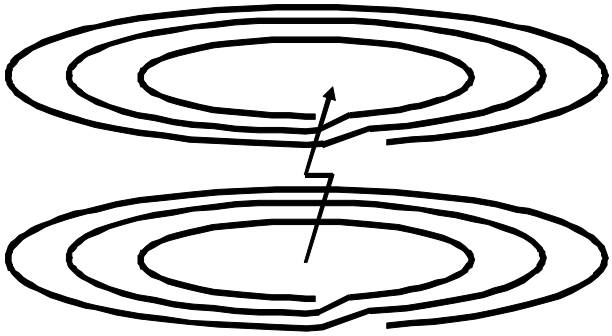

FIGURE 3.3: The planar coil configuration

3.3 PLANAR COILS

Planar coils differs from solenoidal coils in that the loops are all on the same horizontal plane. Figure 3.3 shows a system of two planar coils. Note that each consecutive turn has a smaller diameter than the previous turn, as the turns are placed in the interior of the largest loop. The greatest advantage of planar coils is that, as with single loops, their height is the same as the wire thickness. Unlike single loops and solenoidal coils, however, it is not possible to use the interior of a planar coil, as it is used by the coil itself. Planar coils are also more difficult to manufacture than solenoidal coils or single loops, because all the loops of a planar coil does not have the same diameter. Section 6.3 gives the equations to determine the parameters of a planar coil.

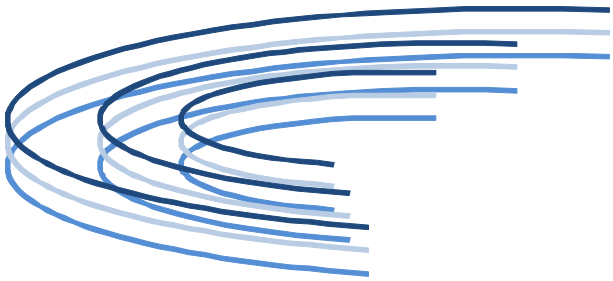

FIGURE 3.4: The hybrid coil configuration. This figure only shows a cut-out of a hybrid coil, in colour code. Each layer is shown in a separate shade of blue.

3.4 HYBRID COILS

In order to increase the coupling coefficient between two coils even more, a hybrid type coil was developed. The coil consists of a vertical array of planar coils, connected in series, as illustrated in Figure 3.4. The hybrid coil is physically the largest of the four types discussed in this section.

It is also the most complex to manufacture, with the highest chance of deviation from the design parameters. The advantage of the hybrid coil is that there are more mutual inductive links than with any other coil types, without having to use more vertical space than solenoidal coils, or using more of the interior than planar coils does. The mathematical background for a hybrid coil will be discussed later in this dissertation, in Section 6.4. In this dissertation, the symbol W will be used to indicate the number of layers in a hybrid coil.

3.5 MIXED COILS

Systems can consist of mixed coil types. In this case the properties of the system will be dependent on the choice of coil types. The ability to mix coil types can be of advantage in situations where either the transmitting coil or the receiving coil must be kept as small as possible. The one coil can then be a single loop, and the other for example a solenoidal coil. Figure 3.5 shows an example of such a system.

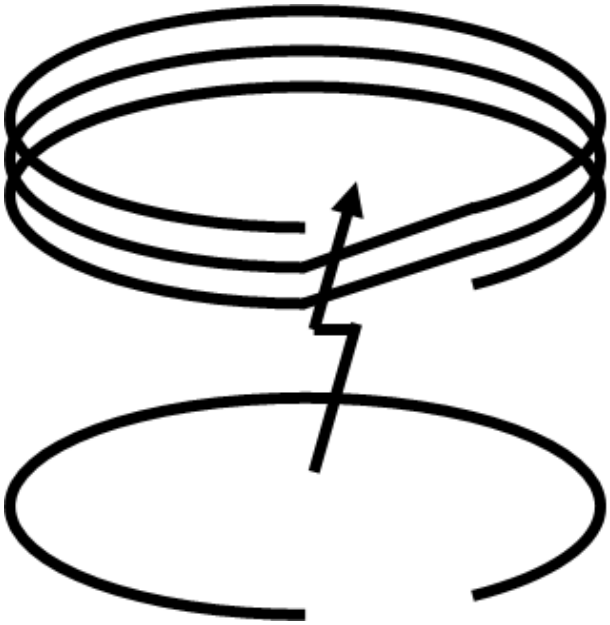

FIGURE 3.5: An example of a mixed coil configuration

3.6 CHAPTER SUMMARY

In this Chapter the coil types that are used in this dissertation are discussed. The coils are discussed in terms of their physical properties and in terms of manufacturing difficulty. Single

TABLE 3.1: A comparison of the different coil types

Coil type	Cost	Complexity	Size
Single loops	Smallest cost	Simplest	Smallest (flat and hollow)
Solenoidal coils	Medium cost	Medium complexity	Larger (vertical)
Planar coils	Medium cost	Medium complexity	Larger (horizontal)
Hybrid coils	Highest cost	Most complex	Largest

loops, solenoidal coils, planar coils and hybrid coils are discussed and compared with each other with focus on their physical size and on manufacturing difficulty. Table 3.1 gives a comparison of the different coil types. The largest part of the wireless power transfer system's cost is the oscillator and the current amplifier. The price range of these chips is about $1 - $5 each. The copper wire is generally in the range of $0.1 per loop.

CHAPTER FOUR

AN OVERVIEW OF MAGNETIC INDUCTIVE POWER TRANSFER

WHEN time-varying electrical current is sent through a loop of wire, a time-varying magnetic field is generated around the loop. This magnetic field can then be used to induce current in another loop of wire within the field. In this way, power is transferred from one loop to the other. An xy-plane view of the magnetic field generated by a loop of wire is shown in Figure 4.1:

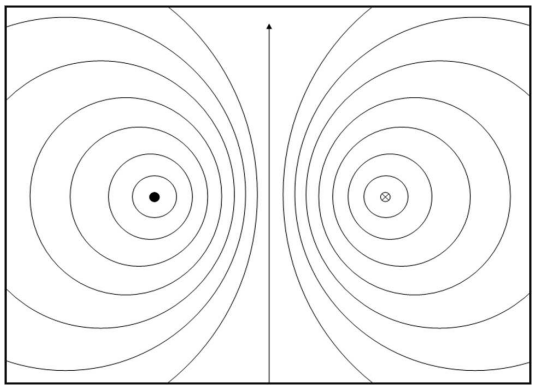

FIGURE 4.1: The magnetic field generated by a loop of wire

At first glance, the system is very similar to a traditional transformer. The system differs from a transformer in that the system does not have a magnetic core, causing very high flux leakage. Another difference is that the distance between the coils is larger than the diameter of the coils. Because the system uses an air-core, the hysteresis losses are eliminated.

4.1 MAGNETIC INDUCTIVE POWER TRANSFER

A magnetic inductive power transfer system consists of a few essential parts as depicted in Figure 4.2:

1. a power source,
2. an oscillator,
3. a tuning capacitor,
4. the transmitter coil,
5. the receiver coil,
6. a tuning capacitor,
7. and a rectifier circuit.

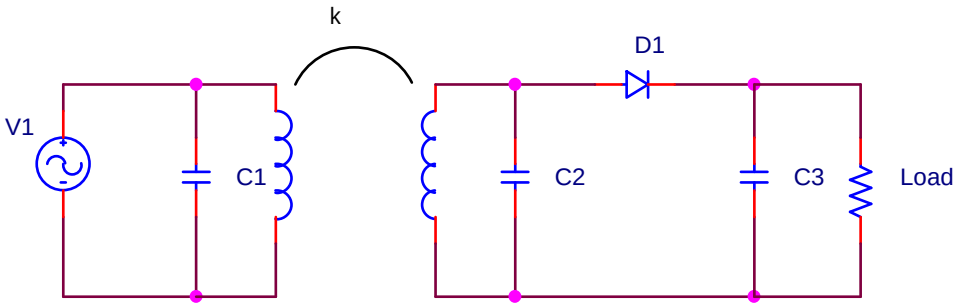

FIGURE 4.2: Circuit of an inductive link

In Figure 4.2 the power source and the oscillator are combined. While a half-wave rectifier is shown to keep the figure simple, a full-wave rectifier would be used in a practical application.

The transmitter and receiver coils are tuned with the tuning capacitors to the frequency of the oscillator. The oscillator develops a sine wave, which is then transmitted by the transmitter coil. At the receiver side the sine wave is received by the receiving coil and rectified to a DC voltage. In this way power is transferred from the transmitter to the receiver. This dissertation will focus on the feasibility of using such a system for transferring power to a wireless sensor node, with special focus on the transmitter and receiver coils. The oscillator and rectifier circuit can be optimized in a number of ways. Cheng *et al* developed a single-stage AC/DC converter with an efficiency of 88%. Their circuit integrates the rectifier and a power-factor-correction

circuit [22]. Schmid *et al* presented a crystal compensated crystal based timer, developed for use in WSNs, which uses two crystals to compensate for each other's drift. This clock can then be amplified with a class-E amplifier, which has more than 95% theoretical efficiency [23].

4.2 EFFICIENCY CONSIDERATIONS

The efficiency of the system is influenced by a few aspects. Firstly, the coupling coefficient, k, influences the efficiency. The coupling coefficient gives an indication of the fraction of the magnetic flux generated by the transmitter coil that is linking the receiver coil. The coupling rate is also important, and gives an indication as to the rate at which flux is linked. Other factors that influence the efficiency are: the radiation resistance of the coils, the absorption resistance of the coils, the oscillator frequency and the operation regime.

For use in a WSN, the efficiency of such a system must be high. The power that is transferred can be very low, in the range of milliwatts, and the distance at which power can be transferred must be larger than the radius of the transmitter coil.

4.3 SAFETY CONSIDERATIONS

In any application that transmits power, safety is an important consideration. If the transmitted power can be received by a human body, the implication is that that power will be dissipated in the human body, with possible harmful consequences. As the human body is a non-magnetic material, its reaction to a magnetic field is small. According to Kangarlu and Robitaille [24] the human body can withstand a specific absorption rate (SAR) of up to 4W/kg without rising the core body temperature to dangerous levels. The transmitter power of a magnetic inductive power transfer system for use in WSNs is expected to be in the milliwatt range, which is much lower than 4W. The greatest danger that must be considered is the proximity of implanted devices such as pacemakers. If the implanted device contains elements with the same oscillation frequency as the magnetic inductive power transfer system, power will be transferred to the implanted device, which can be damaged by the induced power.

4.4 OPERATIONAL REQUIREMENTS

The following operational requirements must be satisfied before magnetic inductive power transfer can be judged as a feasible solution for WSNs:

- The system must be able to transfer power from one device to another over a distance of at least 5 meters, the size of an average office, with an efficiency of at least 8.31%, which allows it to power a MICAz wireless sensor node [25] while transmitting only 1W power, which is within acceptable safety guidelines for a human with minimum weight of 12.5kg, according to the ICNIRP Guidelines [26]. The MICAz wireless sensor node draws 8mA for its processor and 19.7mA for its RF transceiver when in active receiving mode, at a supply voltage of 3V. This adds to a power consumption of 83.1mW, which correspond to 1W transmitted power and an efficiency of 8.31%.

- Neither the transmitter nor the receiver coils should have a diameter of more than 3.2cm, which is the same as the width of a MICAz wireless sensor node [25]. The height of the coils should not be more than 1.4cm, which is the height of a MICAz wireless sensor node without a battery pack.

- The transmitter and receiver should use standard, inexpensive components and should be simple to manufacture. That excludes the use of ferrite materials or litz wire. At about $1 per loop, litz wire is significantly more expensive than solid core copper wire. At $2 - $10 per ferrite core, it adds significant cost to the solution and increases the size of the coils.

4.5 CHAPTER SUMMARY

An overview of the operation, efficiency considerations and the safety considerations of a magnetic inductive power transfer system is given in this Chapter. The operational requirements that are used to judge a system as feasible or not for use in WSNs is given. This Chapter also describes a basic magnetic inductive power transfer system, and gives background knowledge on magnetic inductive power transfer.

CHAPTER FIVE

MID-RANGE POWER TRANSFER IN THE NEAR-FIELD REGION

MOST modern antennae operates in the far-field region, where the electro-magnetic waves are operating in a radiative mode, which entails that much energy is lost in free space. Karalis *et al* [17], investigated mid-range, near-field power transfer. In this type of power transfer, very little power is lost in the surrounding objects and in free space, as both the surrounding objects and free space is off-resonant with the transmitter. The near-fields of the transmitter and receiver overlaps, and is resonant with each other, creating a zone through which power can be transferred efficiently. According to Karalis *et al*, mid-range is the range in which the size of the devices participating in the power transfer is smaller than that of the distance of power transfer by a factor of at least two to three. This will typically be in the order of a few meters. The key characteristics of this type of power transfer are:

- Long-lived oscillatory resonant electromagnetic modes. This means that the resonant structure's intrinsic loss rates, Γ, should be small, i.e. the resonant structure should have a high Q value.
- Resonant coupling. The receiver and transmitter should be tuned to the same resonant frequency.
- Evanescent coupling. Evanescent coupling occurs when the near-fields of the two resonant structures' near-fields overlap.

5.1 COUPLED-MODE THEORY

H.A. Haus [27] presented a coupling-mode formalism that is general and can be applied to magnetic inductive power transfer systems. Karalis *et al* [17] adapted it as follows by introducing loss rates into the Equation:

$$\mathbf{F}(\mathbf{r},t) = a_1(t)\mathbf{F}_1(\mathbf{r}) + a_2(t)\mathbf{F}_2(\mathbf{r}), \tag{5.1}$$

where $\mathbf{F}_1(\mathbf{r})$ and $\mathbf{F}_2(\mathbf{r})$ are the eigenmodes of the two resonant objects. The field amplitudes, $a_1(t)$ and $a_2(t)$ are then given as:

$$\frac{d\mathsf{a}_1}{dt} = -\mathbf{i}(\omega_1 - \mathbf{i}\Gamma_1)\mathsf{a}_1 + \mathbf{i}\kappa\mathsf{a}_2 \tag{5.2}$$

$$\frac{d\mathsf{a}_2}{dt} = -\mathbf{i}(\omega_2 - \mathbf{i}\Gamma_2)\mathsf{a}_2 + \mathbf{i}\kappa\mathsf{a}_1, \tag{5.3}$$

where ω_1 and ω_2 are the respective centre frequencies, Γ_1 and Γ_2 the intrinsic loss rates and κ the coupling rate.

According to Haus and Huang [28], if one of two objects with equal centre frequency is excited, the solution to the system takes the form of the symmetric and antisymmetric combinations of a_1 and a_2. Should the two objects have different centre frequencies, the solutions would acquire the character of the mode to whose frequency the eigenvalue is the closest. Thus, the power transfer between the objects will not be complete. The power transfer efficiency is therefore the highest when the objects have the same centre frequency.

Karalis *et al* [17], further develop this idea by stating that when the two objects are at exact resonance, meaning that when the respective centre frequencies and the loss rates are equal, the energy transfer between the two objects is nearly perfect, except for the losses in the system. The key to efficient energy transfer is thus to keep the coupling rate, κ, much higher than the loss rates, Γ_1 and Γ_2. Therefore, the system will have to operate at high Q values.

Operation at high Q values has advantages and disadvantages. The advantages are that energy transfer will be optimized between the transmitter and the receiver, and interaction with other objects in the vicinity will be minimal. The greatest disadvantage is that high Q values means that the system will have a low bandwidth, which makes the system's manufacturing tolerances appreciably smaller. Because the system is designed for energy transfer and not for information transfer, high bandwidth is not a design requirement. If the bandwidth is too small, however, slight mistuning will lead to serious performance reduction.

Finally, Karalis *et al*'s [17] system requires a high coupling rate. The coupling rate is given as:

$$\kappa = \frac{\omega M}{2\sqrt{L_1 L_2}}, \tag{5.4}$$

where M is the mutual inductance between the coils and L_1 and L_2 are the self-inductances of the respective coils. Because the coupling rate is linear to ω it is possible to increase the coupling rate with frequency. The absorption resistance also increases with frequency because of the skin effect, thereby limiting the maximum frequency.

The coupling rate, as shown in Equation (5.4) is also dependent on the relative relationship of the mutual coupling between the transmitter and the receiver, and the self-inductances of the transmitter and the receiver. In order to obtain a large coupling rate, the mutual inductance between the transmitter and the receiver must be large while the self-inductances remain small.

5.2 EFFICIENCY OF A COUPLED-MODE SYSTEM

The efficiency of a coupled-mode system is given by Karalis *et al* [17] as:

$$\eta = \frac{1}{1 + \frac{1}{\sqrt{1+fom^2}} \cdot \left[1 + \frac{1}{fom^2}\left(1 + \sqrt{1+fom^2}\right)^2\right]}, \tag{5.5}$$

where η is the efficiency and fom is the distance-dependent figure-of-merit of the system. The figure-of-merit of the system gives a rough indication of the system's efficiency, but is much simpler to compute than the efficiency itself. The figure-of-merit of the system is determined with Equation (5.6):

$$fom = \frac{\kappa}{\sqrt{\Gamma_t \Gamma_r}}, \tag{5.6}$$

where Γ_t and Γ_r are the loss rates of the transmitter and receiver, respectively.

Figure 5.1 shows the efficiency of the system against the figure-of-merit. Note that the efficiency of the system increases with the figure-of-merit. A small change in the figure-of-merit can lead to a large change in efficiency. A figure-of-merit of 2 relates to an efficiency of 38%. A figure-of-merit of 3, however, relates to an efficiency of 52%, which is an increase of 14%. This demonstrates how a slight mismatch can detriment system performance drastically.

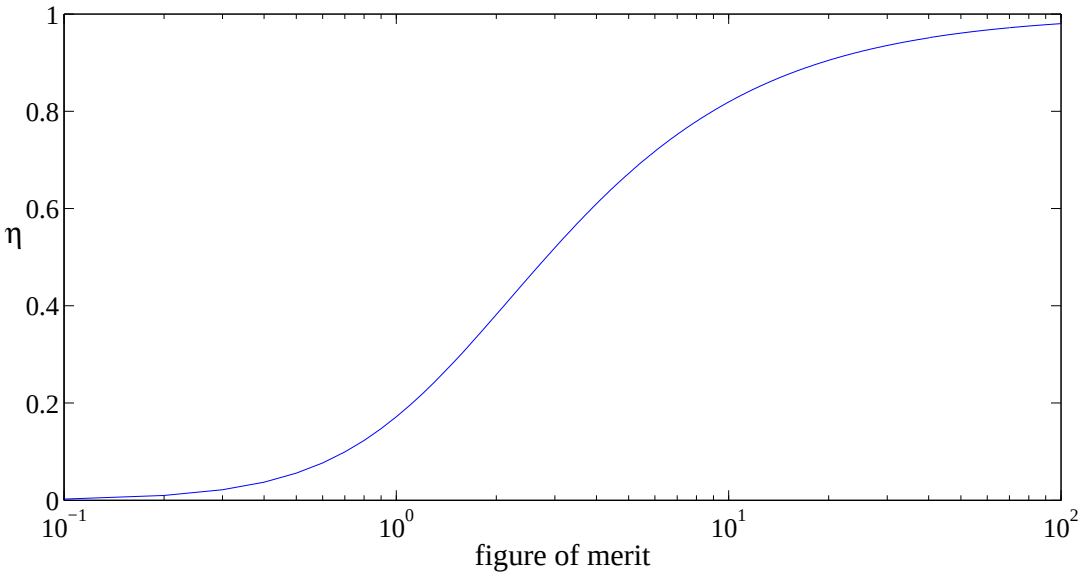

FIGURE 5.1: The efficiency of the system plotted as a function of the figure-of-merit.

In order to obtain maximum efficiency, it is necessary to work in the region where the figure-of-merit is the largest. Figure 5.2 shows the relationship between the frequency of the system and the figure-of-merit.

Figure 5.2 show that the system has a clear optimum frequency. This type of graph can thus be used to determine the optimum frequency for a specific system. Even though the figure-of-merit values of Figure 5.2 are distance dependent, the frequency values are not, meaning that while the system efficiency is dependent on the distance, the optimum frequency is constant over distance. The large bandwidth of Figure 5.2 is misleading as Figure 5.2 is for the case where the receiver and the transmitter are coupled on the same (even if not optimal) frequency. Mis-matching between the receiver and transmitter frequency is a different scenario which is not shown by Figure 5.2.

5.3 DETERMINATION OF THE PARAMETERS FOR A SINGLE WIRE LOOP

This section describes the parameters for a single wire loop. These parameters will be used later in this Chapter as basic building blocks in order to determine the parameters of more complex coil types such as solenoidal coils.

The inductance of a single loop of wire can be determined with the following equation, as

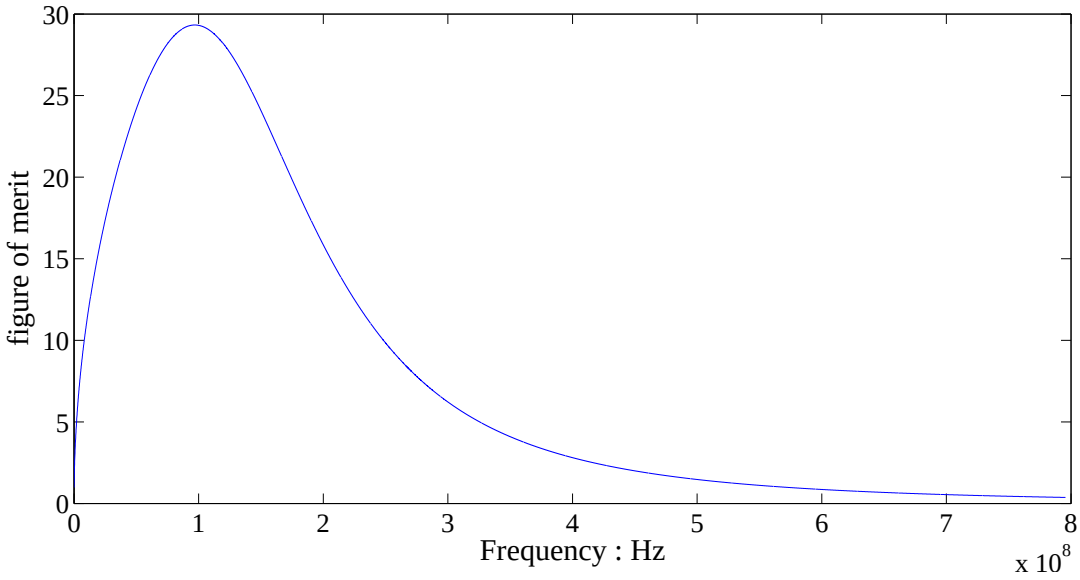

FIGURE 5.2: The figure-of-merit of the system plotted as a function of frequency.

given in Zierhofer and Hochmair [12]:

$$L(a,r) = \mu_0 a \left(\ln\left(\frac{8a}{r}\right) - 2 \right), \tag{5.7}$$

where L is the inductance, a the wire radius and r the loop radius. The resistance of a wire loop consists of two parts: the radiative resistance and the ohmic resistance. The radiative resistance of the loop is given as [29]:

$$R_{rad} = \frac{8}{3}\pi^3 \eta \left(\frac{\pi r^2}{\lambda^2}\right)^2 \tag{5.8}$$

where η refers to the characteristic impedance ($\sim 377\Omega$ for free space) of the medium into which the loop is radiating, r refers to the loop radius and λ is the operating wave length. The ohmic resistance of the loop is given by Karalis *et al* [17] as:

$$R_{abs} \approx \frac{\eta_c r}{a} \tag{5.9}$$

where r is the loop radius, a the wire radius and η_c is given by:

$$\eta_c = \sqrt{\mu_c \omega / 2\rho} \tag{5.10}$$

where μ_c is the permeability of the wire and ρ the conductivity of the wire. Equation (5.9) takes the skin depth into account.

5.4 COUPLED MODE THEORY APPLIED TO SINGLE LOOPS

The inductance, the absorption resistance and the radiation resistance of a single loop were determined in Section 5.3. This Section expands on the parameters determined in Section 5.3 by applying them to the mathematics for energy transfer in the mid-range, strongly coupled region. Although the work closely follows than done by Karalis *et al* [17], the equations used in some cases differs from those used by them, as some of their equations do not give the results that they published.

The resonant frequency of the loop can be determined with Equation (5.11):

$$\omega = \frac{1}{\sqrt{LC}}, \tag{5.11}$$

where C is the parallel tuning capacitor for the loop. For a practical coil the optimum frequency would be obtained with a graph such as shown in Figure 5.2, and then the capacitor value would be obtained. Once the centre frequency of the coil is obtained, the various Q values can be determined [17]:

$$Q^{abs} = \frac{\omega L}{R_{abs}} \tag{5.12}$$

and

$$Q^{rad} = \frac{\omega L}{R_{rad}} \tag{5.13}$$

where Q^{rad} is the radiation Q and Q^{abs} the absorption Q. The total Q of the system can then be determined with the parallel combination of Q^{rad} and Q^{abs}:

$$Q = \left(\frac{1}{Q^{rad}} + \frac{1}{Q^{abs}} \right)^{-1} \tag{5.14}$$

The radiation resistance of a single loop can be determined with Equation (5.15) [29]:

$$R_{rad} = \frac{8}{3}\pi^3 \eta \left(\frac{\pi r^2}{\lambda^2} \right)^2 \tag{5.15}$$

where $\eta = \eta_0$, which is the characteristic impedance of free space. The absorption resistance of the single loop can be determined as follows [17]:

$$R_{abs} = \frac{\eta_{loop} r}{a} \tag{5.16}$$

where η_{loop} is the characteristic impedance of the loop, and is given by:

$$\eta_{loop} = \sqrt{\frac{\mu_c \omega}{2\sigma}} \tag{5.17}$$

with μ_c the permeability of the loop. In the case of copper, it is the same as that of free space. In Equation (5.17), σ refers to the conductivity of the loop, which is $5.998 \times 10^7\ S \cdot m^{-1}$ for copper.

Furthermore, it is necessary to determine the mutual inductance, M, between the two loops. The mutual inductance can be determined with Equation (5.18), as given by Zierhofer and Hochmair [12]:

$$M(r_1, r_2, D) = \mu_0 \cdot \sqrt{r_1 r_2} \left[(\frac{2}{\xi} - \xi) K(\xi) - \frac{2}{\xi} E(\xi) \right] \tag{5.18}$$

where

$$\xi = \left(\frac{4 r_1 r_2}{(r_1 + r_2)^2 + D^2})^{\frac{1}{2}} \right) \tag{5.19}$$

where r_1 and r_2 are the radii of the respective loops. $K(\xi)$ and $E(\xi)$ are the complete elliptic integrals of the first and second kinds, respectively. The coupling rate can then be determined with Equation (5.4). The loss rate of the system can be calculated with:

$$\Gamma = \frac{\omega}{2Q} \tag{5.20}$$

Once the loss rate and the coupling rate of the system are known, the figure-of-merit of the system can be determined with Equation (5.6), and the efficiency of the system with Equation (5.5).

According to [17] the following requirements must be met in order to ensure efficient mid-range power transfer:

- $r << D << \gamma$ to ensure that the system operates in the near-field region, the loop radius must be smaller than the separation distance, which should be smaller than the wavelength.
- $Q^{abs} >> 1000$ and $Q^{rad} >> 10,000$ to ensure that the system operates in the strongly coupled region.
- $\kappa > \Gamma$ - the coupling rate must be larger than the loss rate.

If these requirements are met medium-range, medium-power, power transfer is possible. The greatest difference between this scheme and capacitively-loaded conductive loops which are used in cell phones is that the loops used in cell phones are operating in the far field region, with $D/r >> 1$, and with Q^{rad} designed small to make the antenna efficient for data transfer, rather than for energy transfer.

5.5 COUPLED MODE THEORY APPLIED TO SOLENOIDAL COILS

The important parameters that must be determined in order to apply couple mode theory to other coil types are:

- the coils' self-inductances, which includes the mutual inductances between the coils' turns,
- the mutual inductance between the two coils,
- the coil's absorption resistance,
- and the coil's radiation resistance.

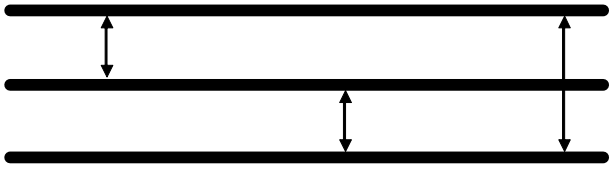

FIGURE 5.3: The mutual inductance on a solenoidal coil

The self-inductance of a solenoidal coil is the sum of all the loops' self-inductances plus the sum of the mutual inductance between all the loops [12]:

$$L_r = \sum_{i=1}^{N_r} L(r_i, a) + \sum_{i=1}^{N_r} \sum_{j=1}^{N_r} M(r_i, r_j, d)(1 - \rho_{i,j}) \tag{5.21}$$

where $\rho_{i,j} = 1$ for $i = j$ and $\rho_{i,j} = 0$ otherwise. The distance between the loops of the solenoidal coil is represented by d. In Equation (5.21), the first part, the summation of $L(r_i, a)$, refers to the loop inductance as determined with Equation (5.7), while the second part, the summation over $M(r_i, r_j, d)(1 - \rho_{i,j})$, refers to the mutual induction between the various loops

as given in Equation (5.18). Figure 5.3 shows a side view of a solenoidal coil. In Figure 5.3 each turn is shown as a single loop, viewed from the side. The arrows shows where the mutual inductances between the turns must be determined.

The mutual inductance between the coils is more complex than the case for single loops, as the mutual inductance between every loop in the one coil, and every loop in the other coil must be determined, as shown in Equation (5.22):

$$M = \sum_{i=1}^{N_r} \sum_{j=1}^{N_r} M(r_i, r_j, D_{ij}) \tag{5.22}$$

where D_{ij} refers to the exact distance between loops r_i and r_j, including the distance between the coils, D, and the small distances between the turns in each coil.

The absorption resistance of a solenoidal coil can be determined by viewing each loop of the solenoidal coil as a series resistor. Adapting Equation (5.16) shows that the absorption resistance of the solenoidal coil is:

$$R_{abs} = \frac{\eta_{loop} r}{a} \cdot N \tag{5.23}$$

The same principal is applied to Equation (5.15) to determine the radiation resistance of a solenoidal coil, which becomes:

$$R_{rad} = \frac{8}{3}\pi^3 \eta \left(\frac{\pi r^2}{\lambda^2}\right)^2 \cdot N \tag{5.24}$$

Once these parameters have been determined, the efficiency of the system can be determined as discussed in Section 5.2.

5.6 COUPLED MODE THEORY APPLIED TO PLANAR COILS

The same parameters that are important to determine for solenoidal coils are important for planar coils. Once the self-inductance, mutual inductance, absorption resistance and the radiation resistance of the coil has been determined, the efficiency of the system can be determined as per Section 5.2.

The self-inductance of a planar coil is simply the sum of the self-inductances of the various loops, added to the sum of the mutual inductances between the loops. As with solenoidal coils, Equation (5.21) can be used to determine the self-inductance of a planar coil. Note that d for Equation (5.21) will be zero, as d refers to the vertical distance between the coils. Instead,

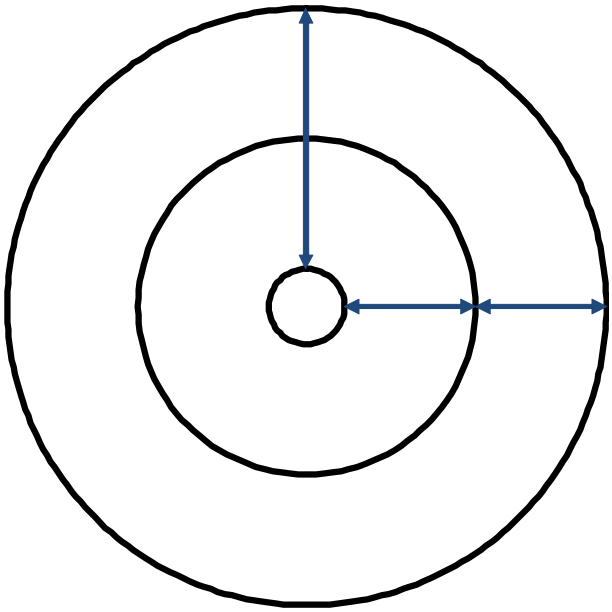

FIGURE 5.4: The mutual inductance on a planar coil

the various radii, r_i and r_j will change. Figure 5.4 shows the mutual inductances between the windings of a $N = 3$ planar coil. Figure 5.4 shows a top view of a planar coil.

The mutual inductance between two planar coils can be determine with Equation (5.22) as is done for solenoidal coils. In this case, the computation to determine the mutual inductance between the two coils is simpler than was the case for solenoidal coils, as the distance between the coils is constant for all the loops, unlike the case of solenoidal coils where the distance between the coils has to take the distance of each loop in the coil from the start of the coil into account.

In order to determine the absorption resistance of a planar coil, Equation (5.16) is adopted to determine the absorption resistance of each of the loops, and to then sum those absorption resistances:

$$R_{abs} = \sum_{i=1}^{N_r} \frac{\eta_{loop} \cdot r_i}{a}. \tag{5.25}$$

The same applies to the radiation resistance; Equation (5.15) is adopted for planar coils. The result is Equation (5.26):

$$R_{rad} = \sum_{i=1}^{N_r} \frac{8}{3}\pi^3 \eta \left(\frac{\pi r_i^2}{\lambda^2}\right)^2. \tag{5.26}$$

5.7 COUPLED MODE THEORY APPLIED TO HYBRID COILS

The self-inductance of a hybrid coil can be determined by adapting Equation (5.21), as for solenoidal coils and planar coils. The most important difference is that care must be taken to determine the mutual inductance between each combination of loops in the hybrid coil. Figure 5.5 shows a wire view of one side of a two layer, three turn, hybrid coil. Each of the large circles represents a wire, while each of the arrows represents a mutual induction. Only one side of the coil is shown.

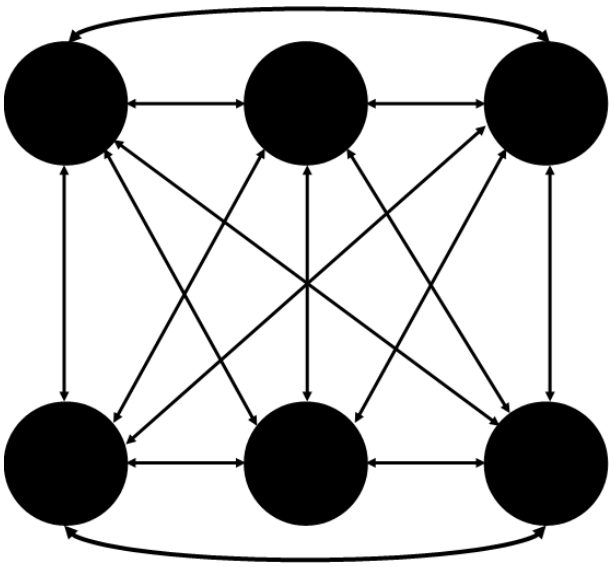

FIGURE 5.5: The mutual inductances on a hybrid coil

Adapting Equation (5.21) for use in hybrid coils gives the following:

$$L_r = \sum_{k=1}^{W}\sum_{i=1}^{N} L(r_{k,i}, a) + \sum_{k=1}^{W}\sum_{l=1}^{W}\sum_{i=1}^{N}\sum_{j=1}^{N} M(r_{k,i}, r_{l,j}, d)(1 - \rho_{i,j,k,l}) \tag{5.27}$$

where $1 - \rho_{i,j,k,l} = 1$ for $[(i = j)\&\&(k = l)]$ and $1 - \rho_{i,j,k,l} = 0$ otherwise. In order to confirm that the correct number of mutual inductance calculations were done, the following equation can be used:

$$calc_{\#} = \frac{(W \cdot N)^2 - (N + W)}{2} \tag{5.28}$$

The mutual inductance between two hybrid coils can be determined by adapting Equation (5.22):

$$M = \sum_{k=1}^{W}\sum_{l=1}^{W}\sum_{i=1}^{N}\sum_{j=1}^{N} M(r_{k,i}, r_{l,j}, D_{ijkl}) \tag{5.29}$$

where D_{ijkl} again refers to the exact distance between the centres of loops r_{ki} and r_{lj}.

The radiation resistance and the absorption resistance of a hybrid coil is determined by summing all the radiation resistances and all the absorption resistances of the individual loops:

$$R_{abs} = \sum_{k=1}^{W}\sum_{i=1}^{N} \frac{\eta_{loop} \cdot r_{k,i}}{a} \tag{5.30}$$

$$R_{rad} = \sum_{k=1}^{W}\sum_{i=1}^{N} \frac{8}{3}\pi^3\eta \left(\frac{\pi r_{k,i}^2}{\lambda^2}\right)^2 \tag{5.31}$$

5.8 CHAPTER SUMMARY

In this Chapter the mid-ranged, near-field, coupled power transfer method of Karalis *et al* is discussed and equations are developed to apply it to the various coil types. The basic principles of coupled-mode theory is discussed. For each coil equations are given to determine the coil parameters such as the mutual inductance, self-inductance, the coupling coefficient and the radiation- and absorption resistances. The main difference between the analyses in this Chapter and that done by Karalis *et al* is that Karalis *et al* applied their analysis only to single loops. In this Chapter the analysis is adapted to the other coil types, and the mathematical background for hybrid coils is developed.

CHAPTER SIX

THEORETICAL COMPARISON OF DIFFERENT COIL TYPES

THE purpose of this chapter is to compare the different coil types theoretically with each other in order to determine which coil type should perform the best. The maximum diameter for the compared coils is 3.2cm, and the maximum allowed height for the coils is 1.4cm, as discussed in Chapter 4.4. The wire diameter is 2mm, which is the maximum diameter solid copper wire which could be obtained inexpensively. Aspects which will be investigated are the:

1. coupling coefficient,
2. self-inductance,
3. mutual inductance,
4. loss rates,
5. coupling rate,
6. and the efficiency according to the coupled mode model of Karalis *et al* [17].

6.1 SINGLE LOOPS

6.1.1 Self-inductance

The self-inductance of a single loop is easy to determine with Equation (5.7). For a single loop of above mentioned parameters, the inductance was determined to be 142.56nH.

6.1.2 Mutual inductance

The mutual inductance of a single loop is determined with Equation (5.18) and Equation (5.19). In order to be able to compare the results between the different coil types, the mutual inductance for a separation distance of $5 \cdot r$ (five times the coil radius) will be given. In the case of a single loop the mutual inductance was determined to be 451.38pH.

6.1.3 Coupling coefficient

The coupling coefficient between two single coils is determined with Equation (2.1) to be 0.0032, which relates to 0.32%. A coupling coefficient of 0.32% is very low, and shows why it is important to work in the resonantly coupled, high Q, region of Karalis *et al* [17] in order to achieve efficient power transfer.

6.1.4 Coupling rate

In order to determine the coupling rate of a system, it is first necessary to determine the operating frequency of the system. This is done by determining for which frequency the fom value, as determined in Equation (5.6) will be highest. Algorithm 1 is used to determine this optimal frequency for a given frequency range. The optimal frequency of the loop is influenced only by its physical parameters. For a single loop system with the given parameters, the optimal frequency is determined as 142MHz. The coupling rate, determined with Equation (5.4) is then $1.41\mu s^{-1}$. It is important to realize that the coupling rate is a combination of how fast energy is transferred in the system, and the coupling coefficient. On its own the coupling rate cannot be used as an indication as to the efficiency of the system.

Algorithm 1 Determining the optimal frequency of the system

for $frek$ = $start\_frequency$ to $end\_frequency$ **do**
  determine $radiance\_resistance$ for $frek$
  determine $absorption\_resistance$ for $frek$
  determine Q for $frek$
  determine fom for $frek$
end for
$high\_fom \Leftarrow$ max(fom)
$opt\_frek \Leftarrow$ lookup($frek$, $high\_fom$)

6.1.5 Loss rate

The loss rate of a single loop is determined with Equation (5.16), Equation (5.15), Equation (5.13) and Equation (5.20). For the single loop system of this example, the loss rate is $40.00/ms$. As with the coupling rate, the loss rate of the system gives an indication as to how fast energy is lost in the system.

6.1.6 Efficiency

Before the efficiency of the system can be determined, it is necessary to determine the figure-of-merit of the system with Equation (5.6). For this system, it is 4, which relates to an efficiency of 57.17% as per Equation (5.5).

6.2 SOLENOIDAL COILS

In order to make comparison between coil types clearer, the coils are limited to $N = 3$ (three turns). The choice of $N = 3$ was made because the differences between the results for the various coil types is clear at $N = 3$, while the difference between the distance between the outer loops of the coils is not yet large enough to be significant. If more turns are added, the efficiency of the coil will increase, though the increase will be less with each added turn, as the distance between the added loops will increase with two times the wire radius.

6.2.1 Self-inductance

The self-inductance of a solenoidal coil is determined with Equation (5.21). To do this, Algorithm 2 was used. The self-inductance of the three turn solenoidal coil is determined as 1.06μH.

6.2.2 Mutual induction

The algorithm to determine the mutual inductance of a solenoidal coil (Algorithm 3) is very similar to Algorithm 2. The mutual inductance of the solenoidal coil is determined with Equation (5.22) as 3.79nH. Algorithm 3 also shows the algorithm used to determine the separation distance between the loops for which the mutual inductance is determined at that moment.

Algorithm 2 Determining the self-inductance of a solenoidal coil

determine $induction\_loop$

$L \Leftarrow induction\_loop \cdot N$

for i = 1 to N **do**

  for j = 1 to N **do**

    if i not equal j **then**

      determine $mutual\_induction_{ij}$

      $L \Leftarrow L + mutual\_induction_{ij}$

    end if

  end for

end for

Algorithm 3 Determining the mutual inductance of a solenoidal coil system

for i = 1 to N **do**

  for j = 1 to N **do**

    $distance \Leftarrow separation + 2 * wire\_radius * ((j-1) + (N-i))$

    determine $mutual\_induction_{ij}$

    $mutual\_induction \Leftarrow mutual\_induction + mutual\_induction_{ij}$

  end for

end for

6.2.3 Coupling coefficient

The coupling coefficient between the solenoidal coils is determined in exactly the same way as for single loops. In this case the coupling coefficient is 0.0036, or 0.36%.

6.2.4 Coupling rate

As with single loops, it is necessary to determine the system's optimal frequency before the coupling rate can be determined. Algorithm 1 is used to determine the optimal frequency. In the case of the solenoidal coil it is 142MHz. The coupling rate, determined using Equation (5.4), is 1.59μs^{-1}.

6.2.5 Loss rate

The loss rate for the solenoidal coil is determined with Equation (5.23), Equation (5.24), Equation (5.13) and Equation (5.20). While similar to the equations used for a single loop system, the radiation resistance and the absorption resistance equations used for a solenoidal coil is different. The loss rate determined for this solenoidal system is 161.18$/ms$.

6.2.6 Efficiency

The figure-of-merit of the solenoidal system, as determined with Equation (5.6), is 10. This corresponds to an efficiency of 81.73%.

6.3 PLANAR COILS

In order to compare with a planar coil, a three turn planar coil with loop diameters of 32mm, 30mm and 28mm was evaluated. A three turn planar coil was used to make the results comparable with those of the solenoidal coil.

6.3.1 Self-inductance

The self-inductance of the planar coil is determined as described in Section 5.6. The self-inductance of the planar coil is determined as 972.80nH by using Algorithm 4.

Algorithm 4 Determining the self-inductance of a planar coil

for i = 1 to N **do**
  determine $self\_inductance_i$
  $L \Leftarrow L + self\_inductance_i$
end for
for i = 1 to N **do**
  for j = 1 to N **do**
    if i not equal j **then**
      determine $mutual\_induction_{ij}$
      $L \Leftarrow L + mutual\_induction_{ij}$
    end if
  end for
end for

6.3.2 Mutual inductance

The mutual inductance of a system of planar coils is determined by using Equation (5.22). The algorithm used to do this is the same as Algorithm 3, except that $distance$, the distance between the coils, is zero for planar coils. Algorithm 3 gives a mutual induction of 3.19nH.

6.3.3 Coupling coefficient

Using Equation (2.1), a coupling coefficient of 0.0033, or 0.33%, is obtained for the planar coil system.

6.3.4 Coupling rate

Using Equation (5.4), a coupling rate of $1.54\mu s^{-1}$ is determined for the planar coil system. The optimum frequency for the system is 150MHz.

6.3.5 Loss rate

Determining the loss rate for the planar coil system is slightly more complicated than for the solenoidal system. Equation (5.26), Equation (5.25), Equation (5.13) and Equation (5.20) are used to determine the loss rate for a planar coil system. Algorithm 5 applies these equations. A loss rate of $169.84/ms$ is determined using Algorithm 5.

Algorithm 5 Determining the loss rate of a planar coil

for i = 1 to N **do**

determine $radiation\_resistance_i$

determine $absorption\_resistance_i$

$rad\_res \Leftarrow rad\_res + radiation\_resistance_i$

$abs\_res \Leftarrow abs\_res + absorption\_resistance_i$

end for

determine Q_rad

determine Q_abs

$Q \Leftarrow Q\_rad || Q\_abs$

determine $loss\_rate$

6.3.6 Efficiency

The figure-of-merit of the planar coil system is determined to be 8, while the efficiency of the planar coil system is determined as 80.32%.

6.4 HYBRID COIL

In order to compare the hybrid coil to solenoidal coils and to planar coils, a three turn, three layer hybrid coil is evaluated.

6.4.1 Self-induction

The self-induction of a hybrid coil is determined with Equation (5.27). In order to do the calculations, Algorithm 6 is used. The self-inductance of the hybrid coil is determined as 7.60μH.

6.4.2 Mutual induction

Algorithm 7 is based on Equation (5.29), and is used to determine the mutual induction between two hybrid coils. The mutual inductance for the hybrid coil system is determined as 26.84nH. Algorithm 7 also shows how to determine the distances between the coils.

Algorithm 6 Determining the self-inductance of a hybrid coil

for i = 1 to N **do**
  determine $induction\_layer_i$
  $L \Leftarrow L + induction\_layer_i$
end for
$L \Leftarrow L \times number\_layers$
for k = 1 to $number\_layers$ **do**
  for l = 1 to $number\_layers$ **do**
    for i = 1 to N **do**
      for j = 1 to N **do**
        if (i not equal j) OR (k not equal l) **then**
          $distance \Leftarrow (\textbf{abs}((k-l)) * 2 \cdot a)$
          determine $mutual\_induction_{i,j}$
          $L \Leftarrow L + mutual\_induction_{i,j}$
        end if
      end for
    end for
  end for
end for

Algorithm 7 Determining the mutual inductance of a hybrid coil

for y_bottom = 1 to $number\_layers$ **do**
  for x_bottom = 1 to N **do**
    for y_top = 1 to $number\_layers$ **do**
      for x_top = 1 to N **do**
        $distance \Leftarrow (D + 2 \cdot a \times ((y_top - 1) + (number\_layers - y\_bottom))$
        determine $mutual\_induction_{x\_bottom,x\_top}$
        $M \Leftarrow M + mutual\_induction_{x\_bottom,x\_top}$
      end for
    end for
  end for
end for

6.4.3 Coupling coefficient

The coupling coefficient for the hybrid coil is computed to be 0.0035, or 0.35%.

6.4.4 Coupling rate

The optimum frequency for the hybrid coil system is 150MHz, with a coupling rate of 1.66μs^{-1}.

6.4.5 Loss rate

The loss rate of the hybrid coil system is determined with Equation (5.30), Equation (5.31), Equation (5.13) and with Equation (5.20). Algorithm 8 was written to determine the loss rate of the hybrid coil system, which was found to be 65.19k$/ms$.

Algorithm 8 Determining the loss rate of a hybrid coil

for i = 1 to N **do**
  determine $rad\_res(loop_i)$
  determine $abs\_res(loop_i)$
  $rad\_res \Leftarrow rad\_res + rad\_res(loop_i)$
  $abs\_res \Leftarrow abs\_res + abs\_res(loop_i)$
end for
$rad\_res \Leftarrow rad\_res \times num\_layers$
$abs\_res \Leftarrow abs\_res \times num\_layers$

6.4.6 Efficiency

The figure-of-merit for the hybrid coil system is 26, while the efficiency is 92.46%.

6.5 THEORETICAL COMPARISON

In this section the various coil types are compared with each other. Table 6.1 gives a summary of the key parameters of each coil type.

The theoretical results show that of all coil types, the hybrid coils is the most efficient. The trade-offs, however, are that the hybrid coil is physically the largest of all the coils that were investigated and that the hybrid coil is the most complex to manufacture. The single loop

TABLE 6.1: The key parameters of each coil type

	Single loop	Solenoidal	Planar	Hybrid
Self inductance	142.56nH	1.06μH	972.80nH	7.60μH
Mutual inductance	451.38pH	3.79nH	3.19nH	26.84nH
Coupling coefficient	0.32%	0.357%	0.33%	0.354%
Centre frequency	142MHz	142MHz	150MHz	150MHz
Coupling rate	1.41μs^{-1}	1.59μs^{-1}	1.54μs^{-1}	1.66μs^{-1}
Loss rate	40$/ms$	161.18$/ms$	169.84$/ms$	65.19$/ms$
Efficiency	57.17%	81.73%	80.32%	92.46%

system is the least efficient, which is to be expected because it has only one mutual inductive link between the transmitter and the receiver. The solenoidal coil, which uses three times more wire than the single loop, is 1.4 times as efficient as the single loop. The planar coil, though less efficient than the solenoidal coil, is much more efficient than the single-loop. The difference in efficiency between the planar coil and the solenoidal coil is not much, only ≈ 1.4% in this case. In cases where the device height is limited, it might thus be preferable to use a planar coil rather than a solenoidal coil. Unless the inside of the planar coil is used for other devices, more turns can be added without any significant contribution to the coil size. A four turn planar coil, with an outer loop radius of 3.2cm would have an efficiency of 83.70%, which, while the coil size is not appreciably larger than a three turn coil, and only a third of the height of a three turn solenoidal coil, is 2% more efficient than the three turn solenoidal coil.

An interesting observation is that the optimum frequencies of the single loop and that of the solenoidal coil are the same, while the same applies to the planar coil and the hybrid coil.

The coupling coefficient of the hybrid coil is 0.00354, which is 0.00003 smaller than that of the largest coupling coefficient, which is that of the solenoidal coil. This indicates that the hybrid coil should give similar performance than the solenoidal coil, even in non-resonant, non-evanescent coupling.

Although the optimal operating frequencies for these coils are larger than 100MHz, they are still small enough that inexpensive, readily obtainable commercial components can be used for the oscillator and the power amplifier of the transmitter.

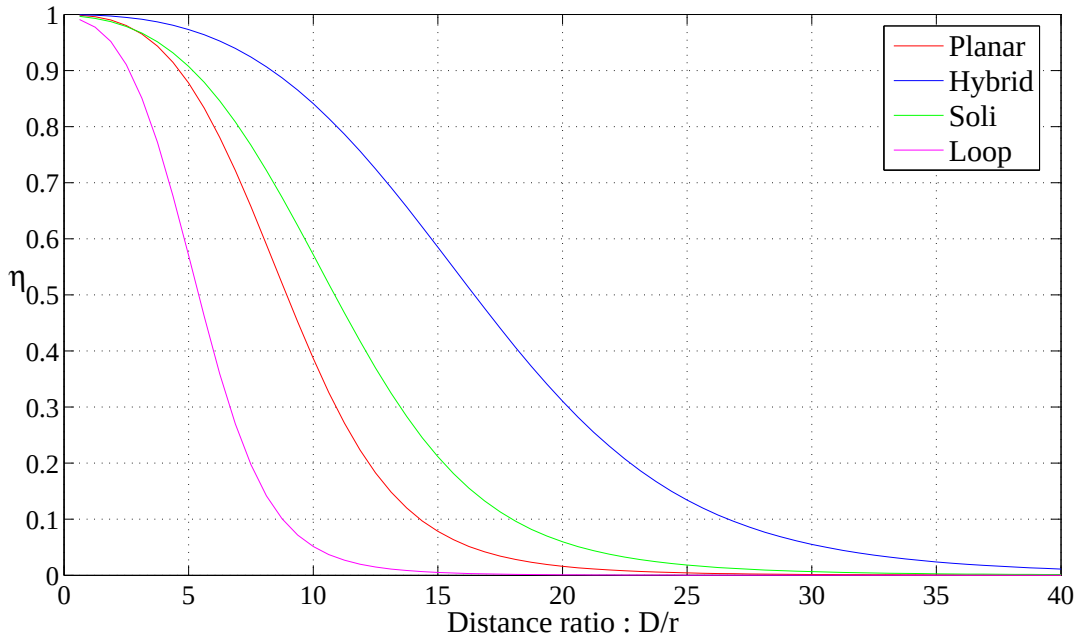

FIGURE 6.1: The optimal efficiencies

6.6 OPTIMAL CASE

In this Section the largest coil that will fit into the constraints of Section 4.4 is discussed. Whereas the previous Sections of this Chapter focussed on comparing various coil types with each other, this Section focuses on the best possible coil that can be created within Section 4.4's constraints. Given a wire radius of 1mm and the design constraints, the largest number of turns that can be fit into a hybrid coil is 10 turns, with a total of 7 layers. Figure 6.1 shows the efficiencies for the optimal configuration within the design constraints of Section 4.4 for each of the coil types.

According to the requirements listed in Section 4.4, the system must be able to transfer power over a distance of 5 meters with an efficiency of at least 8.31%. This correlates to a distance of $D = 312 \cdot r$. The efficiency of the hybrid coil, which is the best performer, is smaller than 8.31% after a distance of $D = 31 \cdot r$, showing clearly that the efficiency of the hybrid coil is going to be much less than 8.31% at a separation distance of 5 meters. The required efficiency of 8.31% is only achieved up to about $D = 31 \cdot r$, which correlates to a separation distance of $D = 0.49$m.

6.7 CHAPTER SUMMARY

The four coil types are compared theoretically with each other in this Chapter. The coil types are discussed in terms of loss rates, coupling coefficients, self- and mutual inductances and efficiencies. The optimal case, where the coil sizes are as large as allowed by the requirements of Section 4.4, is discussed and the maximum separation distance is determined. The results show that the hybrid coil outperforms the other coil types.

CHAPTER SEVEN

EXPERIMENTAL IMPLEMENTATION

THIS chapter discuss an experimental implementation of inductive power transfer systems in order to investigate the various coil types as discussed in previous chapters. The aims of the experimental investigation are to verify the theoretical results of Chapter 6 and to investigate practical considerations and difficulties with inductive power transfer systems.

7.1 REQUIREMENTS

In order to manufacture and obtain results for the theoretical setup there are additional requirements to those for WSNs. The requirements for the theoretical setup are as follows:

- the coils must be of equal size,
- the coils must operate at frequencies for which measurements can be taken with available equipment,
- for safety reasons and as a general precaution the coils must be driven with a low-power source,
- and the test setup must be inexpensive and simple to manufacture and assemble.

7.2 DESIGN

Figure 7.1 shows a block diagram of the experimental setup. The experimental setup consists of three basic parts, which will be discussed shortly in this section:

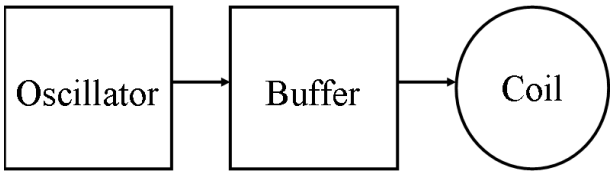

FIGURE 7.1: The experimental setup used to verify the theoretical results.

- an oscillator, which generates a sine wave at the oscillation frequency,
- a buffer, which is capable of supplying more current than the oscillator,
- and the various coils.

7.2.1 Oscillator

The oscillator used for this experimental setup has a frequency range of 70MHz - 130 MHz. The oscillation frequency can be changed with a variable resistor. The oscillator's output is a sine wave, with an amplitude which is dependent on the oscillation frequency.

7.2.2 Buffer

The experimental setup's buffer is an opamp with a maximum current output of 190mA, an output voltage swing of up to $\pm$4V and an operation frequency of up to 220MHz. The maximum power output of the buffer is thus less than 1W.

7.2.3 Coils

Two examples of each of the four coil types were created: single loops, solenoidal coils, planar coils and hybrid coils. The coils has a radius of 4.9cm. Although larger than would be used in a commercial application, this radius was chosen as it is the smallest for which measurements could be taken using available equipment. It is still applicable to the investigation as it tests the theoretical results and is in the same order as would be used in a commercial application. The effect of the larger test coil radius on the efficiency, as long as the D/r ratio is kept constant, is less than 2.5%. The wire radius is 1mm, which is the thickest wire that could be obtained inexpensively. The solenoidal and planar coils have three turns, while the hybrid coils has two layers of three turns.

In the solenoidal coils a separation of 2mm was included between the turns of coil. The same applies to the layers of the hybrid coils. The reason for this separation is manufacturing tolerances which do not allow the turns to be placed immediately next to each other.

7.3 MEASUREMENT METHOD

In order to determine the efficiency of each system, the following method was used:

An 1.2Ω resistor was connected in parallel to the receiver coil. The voltage over the resistor was measured, and the received power was determined with the following equation:

$$P_{received} = \frac{V^2}{R}, \tag{7.1}$$

where R is the 1.2Ω resistor and V is the voltage over the resistor.

Another 1.2Ω resistor was connected in series to the transmitting coil. The voltage over the resistor was measured and used to determine the current in the resistor, which is also the current in the coil because the two are connected in series. The voltage over the coil itself was measured, and the power dissipated in the transmitter was determined with $P_{transmitted} = V \cdot I$. The efficiency of the system was then determined as:

$$\eta = \frac{P_{recieved}}{P_{transmitted}} \tag{7.2}$$

This process was followed for various distances up to $2 \cdot r$, after which the efficiency became too small to be measured accurately.

In order to increase the accuracy of the measurements only one probe was used at a time. The use of two probes causes coupling between the probes, which makes the measurements less accurate. In order to determine the phase difference between the current through the transmitter resistor and the voltage over the transmitter, it was necessary to use two probes. The transmitter current and voltage were found to be in phase with each other, giving an unity power factor. If the true power factor should differ from the measured power factor due to coupling between the probes, the power factor will decrease, meaning that the transmitted power will be less than determined, which will cause the real efficiency to be higher. The efficiency measurements given in this dissertation are for a unity power factor, and are thus rather too small than too large. The power factor for the receiver is unity because the load resistor is in parallel with the coil.

An important consideration when taking the measurements is that all the PCB traces, power cables, device pins and even the probe cables are acting as antennae. Because the current in the power cables oscillates at the centre frequency of the system, the power cables are strongly coupled to the probe cables. Although this coupling consists primarily of electric fields, and is not capable of carrying much power, it is sufficient to make accurate measuring very difficult and to influence the measurements to a large extent. The following steps were taken to compensate for the coupling between the probe cables and the other devices and cables in the system:

- The power supply lines were kept as far away from the probes as possible.
- Where possible, the probe cables were kept perpendicular to the transmitter, in order to minimize the coupling of the probe cables with the transmitter.
- The probe cables were kept straight in order to minimize internal coupling in the probe cables.
- The loop created by the probe and the ground wire of the probe was kept as small as possible.
- The geographic setup of the experiment was kept in such a way that the power cables enters the PCB from the opposite side than the receiver coil and the oscilloscope. The consequence of this is that the induced fields in the cables when taking measurements for the transmitter will be stronger than those when taking measurements for the receiver. The measurements are thus smaller than the real value, rather than larger.

Each measurement was taken at least three times, and only measurements within 10% of each other were accepted. In cases where measurements fell outside the 10% criteria, the cause of the discrepancy was investigated, corrected, and the measurement was taken again. Measurements were also taken on various days.

7.4 THEORETICAL RESULTS FOR THE TEST SETUP

In order to compare the test setup results with theoretical results, coils with the dimensions of the physical coils were investigated theoretically. Table 7.1 shows the theoretically determined self-inductances, coupling coefficients and efficiencies for the test coils. These results takes the 2mm separation due to manufacturing tolerances into account.

TABLE 7.1: The theoretical results for the test coils

Coil type	Self-inductance	Coupling coefficient	Efficiency
Single loop	216.68nH	0.029	93.6%
Solenoidal	1.60μH	0.030	97.2%
Planar	1.71μH	0.031	97.4%
Hybrid	5.37μH	0.033	98.5%

7.5 MEASURED INDUCTANCES

The measured inductances for the various test coils are shown in Table 7.2.

TABLE 7.2: The measured results of the the test coils

Coil type	Self-inductance	Coupling coefficient	Efficiency
Single loop	n.a.	0.026	2%
Solenoidal	1.8μH	0.042	4.1%
Planar	1.4μH	0.043	5.3%
Hybrid	5.3μH	0.044	8.8%

The self-inductance of the single loop could not be measured because it is out of range (too small) of the multi-meter that was used to measure the inductances. All the measured values are in good agreement with the theoretical values, as shown in Tables 7.1 and 7.2. All the measured self-inductances are within 20% accurate with regard to the theoretical inductances. The differences between the experimental results and the mathematical results can be attributed to manufacturing tolerances and the wire core radius variation.

The measured self-inductance values show that the theoretical inductance equations are correct. As the solenoidal, planar and hybrid coil equations use the same principal for the mutual inductance part of the self-inductance than is used for the mutual inductance between two coils, it is safe to assume that the mutual inductance equations are also correct.

7.6 COUPLING COEFFICIENTS

In order to verify the measured coupling coefficients, theoretical simulations were done to compare, for each coil type, the coupling coefficient with the separation distance between the two coils. These results are shown in Figure 7.2.

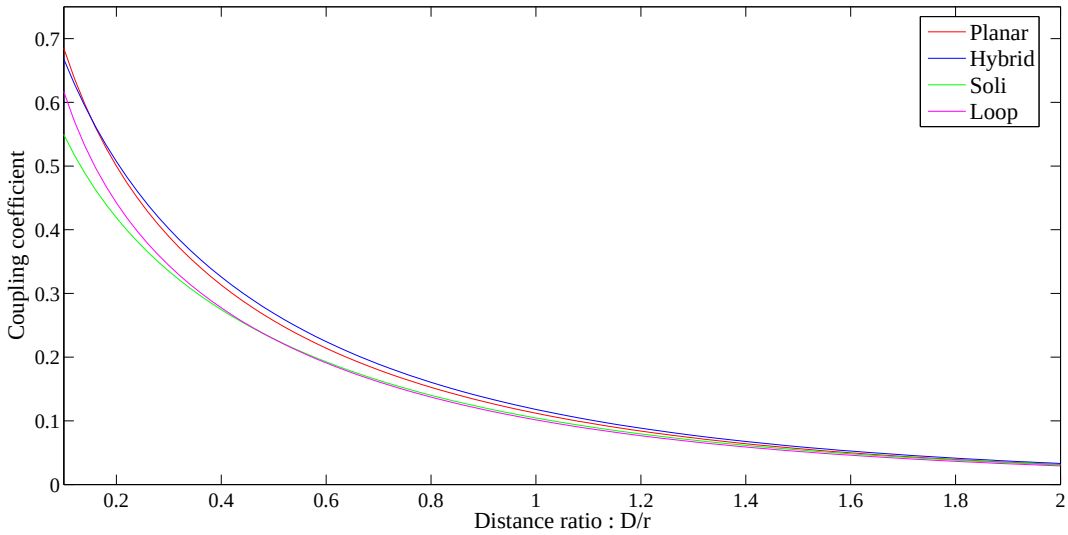

FIGURE 7.2: The theoretically determined coupling coefficients as a function of distance.

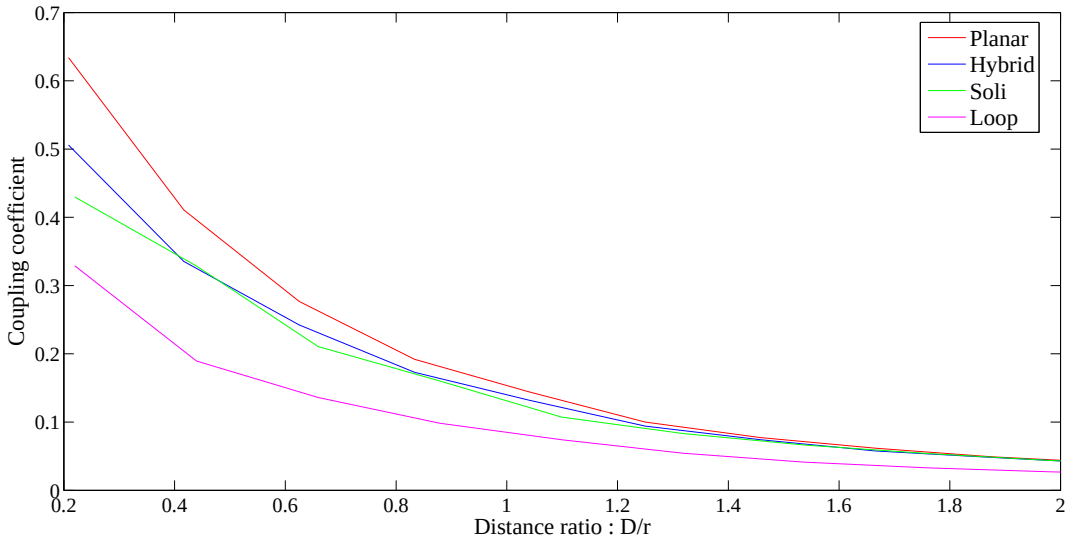

FIGURE 7.3: The experimentally determined coupling coefficients as a function of distance.

The experimental results show good correlation with the theoretical results. The most important differences between the experimental results and the theoretical results are that the theoretical single loop coupling coefficient is much closer to those of the other loops than that of the experimental results is. Also, the theoretical coupling coefficient for the planar coil is smaller than that of the hybrid coil for distances larger than $D/r = 1.53$, while the coupling coefficient of the planar coil for the experimental results is always larger than that of the hybrid coil. The reason for the larger coupling coefficient of the planar coil can be found in the self-inductance of the planar coil which is measured to be significantly smaller than the theoretically determined value. As the coupling coefficient is given by:

$$k = \frac{M}{\sqrt{L_t L_r}}, \tag{7.3}$$

the coupling coefficient of the planar coil will increase for a decrease in self-inductance. For distances larger than $D/r = 2$ the coupling coefficients becomes very close to each other for the various coil types.

7.7 EFFICIENCIES

As with the coupling coefficients, the efficiencies are compared with theoretically determined efficiencies. Figure 7.4 shows the theoretically determined efficiencies of the coils for distances up to $D/r = 20$. Figure 7.5 shows the measured efficiencies of the coils for distances up to $D/r = 2$.

The theoretical efficiencies of the coils are very high and very close to each other, because the separation distance of the coils where the measurements for Table 7.1 was taken was only $D/r = 2$. For strongly coupled, magnetic resonant power transfer, as described by Kurs *et al.* [2], $D/r = 2$ is a short separation. Figure 7.4 shows that the efficiencies of the various coils differs greatly from $D/r = 4$ to $D/r = 12$, after which they decay separately.

The measured efficiencies shown in Figure 7.5 decays much faster than the theoretically determined efficiencies shown in Figure 7.4. The measured results shows that the hybrid coil is the most efficient, followed by the planar coil, the solenoidal coil and finally the single loop, as is also shown by the theoretical results.

The difference between the experimental results and the theoretical results is very large. This suggests that either the theoretical model in Karalis *et al* [17] is faulty, or that the experimental coils are not operating in the mid-range, near-field region required for the their theoretical

model. As the theoretical model of Karalis *et al* [17] has been verified experimentally in Kurs *et al* [2], it will be assumed that the coils are not operating on resonance. This assumption will be investigated in Chapter 8.

7.8 COIL TUNING

In the previous Section, there was a large discrepancy between the experimental efficiencies and the theoretical efficiencies. In order to validate the theoretical model, the single loop coil was fine tuned by hand to resonance. Tuning involved physically stretching and bending the single loop coil. The results obtained using this method are shown in Figure 7.6.

The results of the fine tuned coil are much better those for the coils in Section 7.7. This highlights the importance of operating the coils in the resonant region. While the experimental efficiencies for the single loop coil is still much lower than the theoretical efficiencies, the results in this Section follows the theoretical efficiencies much closer than in Section 7.7.

In the case of the single loop coil, it was possible to fine tune the coil as it consists only of one loop. For the other coils, fine tuning did not work as the coils consist of multiple loops. In order to get the coils on resonance, the manufacturing of the coils needs to be very precise. High quality wire should be used, where the diameter of the wire is constant. The copper wire used in these experiments was found to have a diameter tolerance of up to 50%. Coils will also need to be manufactured in such a way as to ensure that the various loops of the two coils are all the same size.

7.9 CONCLUSION

In this Chapter, the different coil types were investigated experimentally. It was found that the experimental inductances and coupling coefficients shows good correlations with the corresponding theoretical values. The practical efficiencies, however, was found to be much smaller than the theoretical efficiencies. The reason for this is that the coils are not operating on resonance with each other. This phenomenon is discussed in more detail in Chapter 8. After fine tuning, however, the single loop coil showed efficiency comparable with the theoretical results.

At large distances the planar coil has the best experimental coupling coefficient. The coupling coefficient of the single loop is significantly smaller than any of the other coils'

coupling coefficients. The experimental results shows that the efficiency of the hybrid coil is higher than that of any of the other coil types when not operating on resonance. The single loop has the smallest efficiency of all the coil types.

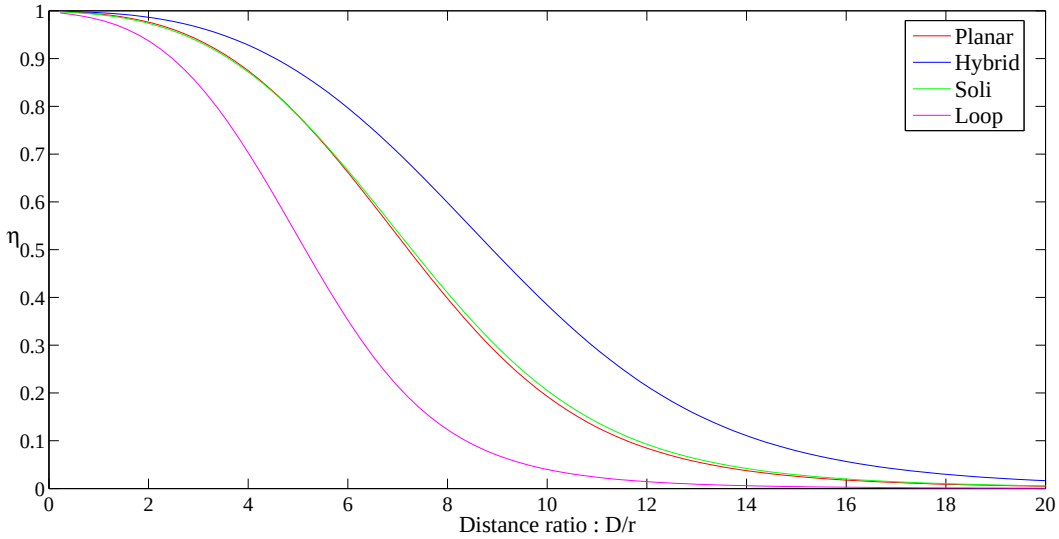

FIGURE 7.4: The theoretically determined efficiencies as a function of the distance

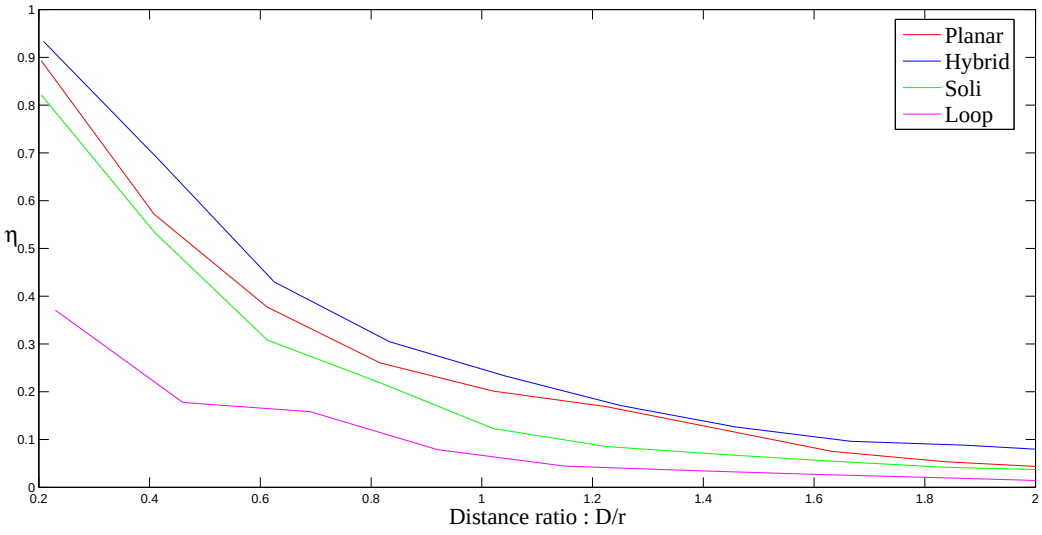

FIGURE 7.5: The experimentally determined efficiencies as a function of the distance.

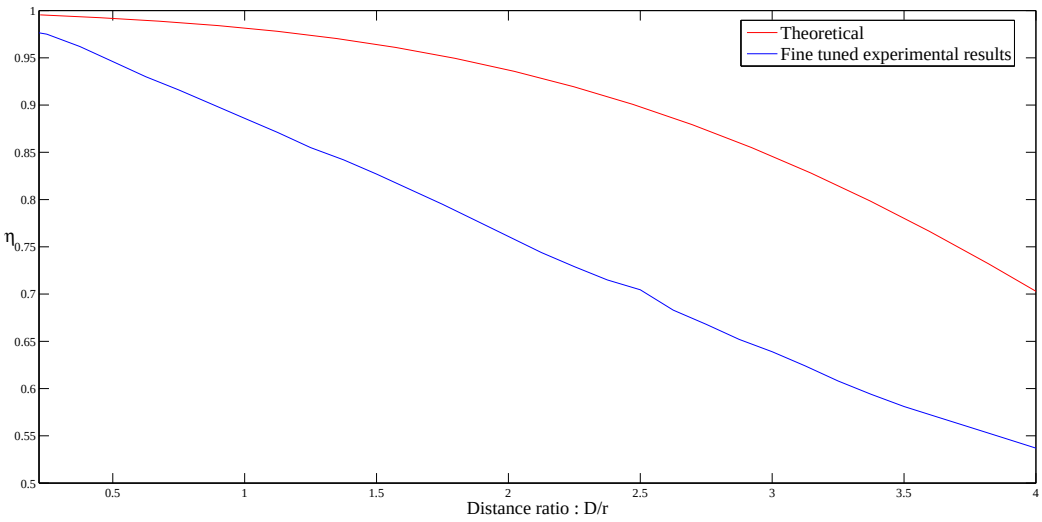

FIGURE 7.6: A comparison of the experimental theoretical efficiencies of a fine tuned single loop coil.

CHAPTER EIGHT

PARAMETER TOLERANCE INVESTIGATION

THE aim of this chapter is to investigate the effect of tolerance issues in the resonant power transfer scheme. The effect of operating the coils off resonance is investigated, as well as the effect of misaligning the coil centres. The effect of the wire radius on the system efficiency is investigated.

8.1 OFF-RESONANCE OPERATION

8.1.1 Theoretical background

According to Kurs *et al* [2], it is '...essential that the coils be one resonance for the power transfer to be practical.' They have found experimentally that the efficiency of the system drops sharply as either of the coils is detuned from resonance. In order to verify this phenomenon theoretically, Equation 8.1 from Haus [27] was used:

$$\mathsf{a}_1(t) = \left[\mathsf{a}_1(0)\left(cos(\Omega_0 t) - j\frac{\omega_2 - \omega_1}{2\cdot\Omega_0}sin(\Omega_0 t)\right) + \frac{\kappa_{12}}{\Omega_0}\mathsf{a}_2(0)sin(\Omega t)\right]\cdot \exp j[(\omega_1+\omega_2)/2]t, \tag{8.1}$$

where ω_1 and ω_2 are the centre frequencies of the respective coils, a_1 and a_2 are the starting amplitudes of the signals on the coils, κ_{12} is the coupling coefficient between the two coils, and Ω_0 is given by:

$$\Omega_0 = \sqrt{\left(\frac{\omega_1 - \omega_2}{2}\right)^2 + |\kappa_{12}|^2}. \tag{8.2}$$

Equation 8.1 does not take the loss rates of the coils into account, it only gives an indication as to the effect of frequency mismatches between the two coils. Equation 8.1 is basically one of the two equations that forms a nontrivial solution to Equation 5.1, with loss rates of zero.

8.1.2 Algorithm

In order to determine the effect of detuning one of the coils from the centre frequency, Algorithm 9 was written. Because the amplitude of the signal is time dependant, Algorithm 9 computes the time at which the signal would be at a maximum for each given frequency as per Equation 8.3:

$$t = \frac{\pi}{2 \cdot \Omega_0} \tag{8.3}$$

Algorithm 9 An algorithm to investigate the effect of detuning the coils from each other.

$freq_2 \Leftarrow$ constant
for $freq_1$ = $start\_freq$ to $stop\_freq$ **do**
  determine $optimum\_time$
  determine a_1 for $freq_1$ and $freq_2$
end for

8.1.3 Simulation results

The setup used for Algorithm 9 is as follows: $\mathsf{a}_2(0) = 0$, $\mathsf{a}_2(0) = 5$ (any $\mathsf{a}_2(0) > 0$ can be used), with a arbitrary small coupling rate κ. Figure 8.1 shows the percentage of power transferred from the transmitter coil to the receiver coil if the frequency of the receiver coil is detuned from that of the transmitter coil. The results are shown in percentage while the frequency is shown as the fraction of the receiver frequency of the transmitter frequency.

8.1.4 Discussion

Figure 8.1 shows the impact of decoupling on the energy transfer. For a fractional decoupling of 5% the attenuation is 37%, for a fractional decoupling of 10% the attenuation is 62%, and for a fractional decoupling of 20% the attenuation is 80%. The severe efficiency degradation of the system correlates with the very small measured efficiencies of Chapter 7.7. Figure 8.1 clearly

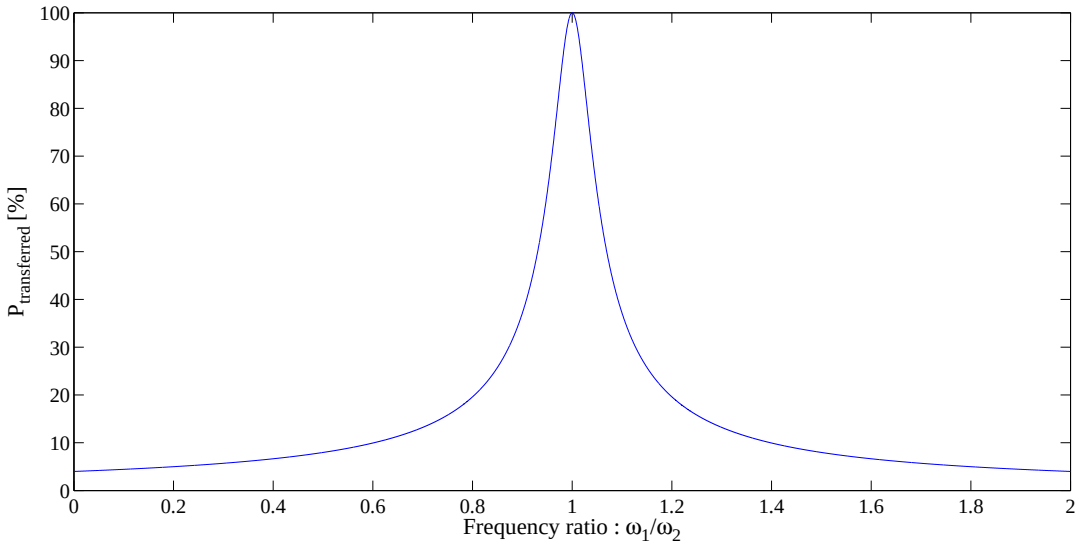

FIGURE 8.1: The efficiency of the system as a function of the decoupling between the coils.

shows the importance of operating at exact resonance for this power transfer scheme. The efficiency degradation is very large for only a small fractional decoupling. In the experimental setup used for Chapter 7 the fractional decoupling can be fairly large because of a number of factors: the tuning capacitors used has a 5% tolerance, the coils were hand-wound, meaning that their tolerances are very large, and the wire used to create the coils is not high quality wire, meaning that the wire radius is not uniform, which also influences the self-inductance and hence the centre frequency of the coil.

In an attempt to confirm the validity of Figure 8.1, the corresponding author of [2] was contacted. The author responded [30] that the coils needed to be on exact resonance and that he agrees that the size of the coils provides a too low achievable efficiency for the application.

8.2 MISALIGNED COIL CENTRES

This section discusses the effects of coil centres that are misaligned. Figure 8.2 shows an example of two single loops that are misaligned. The separation between the centres of the loops is donated by p in the figure.

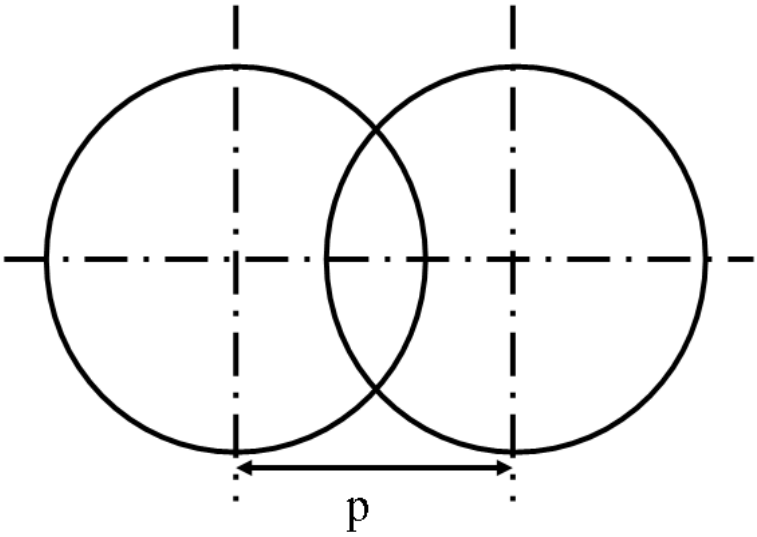

FIGURE 8.2: A figure to demonstrate misalignment between two single loops.

8.2.1 Theoretical background

Equation 5.18 is derived from Equation 8.4 for the special case of $\rho = 0$. Equation 8.4 is given in Zierhofer and Hochmair [12] for the determination of the mutual inductance between two loops:

$$M(r_1, r_2, \rho, D) = \pi\mu_0\sqrt{r_1 r_2}\int_0^\infty J_1\left(x\sqrt{\frac{r_1}{r_2}}\right) J_1\left(x\sqrt{\frac{r_2}{r_1}}\right) J_0\left(x\frac{\rho}{\sqrt{r_1 r_2}}\right) exp\left(-x\frac{D}{\sqrt{r_1 r_2}}\right) dx, \tag{8.4}$$

where J_0 and J_1 are the Bessel functions of the zeroth order and of the first order, respectively. Integration over the product of Bessel functions is a computationally intensive task, especially as each Bessel function itself is an integral. In order to use Equation 8.4 a Matlab function written by Van Deun and Cools was used [31]. The function computes the integral of the product of a number of Bessel functions and of an exponential function. The function was verified by determining a number of mutual couplings using standard integration and comparing the results with those obtained using the function.

8.2.2 Algorithm

Algorithm 10 was used to investigate the effect of the displacement, ρ between the axis.

Algorithm 10 An algorithm to determine the effect of the displacement between the axis of the coils.

determine self-inductances
determine loss rates
for ρ = $start\_pos$ to end_pos **do**
  determine mutual inductances
  determine efficiencies
end for

8.2.3 Simulation results

The distance between the coils used in Algorithm 10 is $D = 2r$, where r is the maximum radius of the coil. Figure 8.3 shows the effect of the displacement between the centres of the coils on the efficiency. Figure 8.4 shows the effect of the displacement on the coupling coefficient.

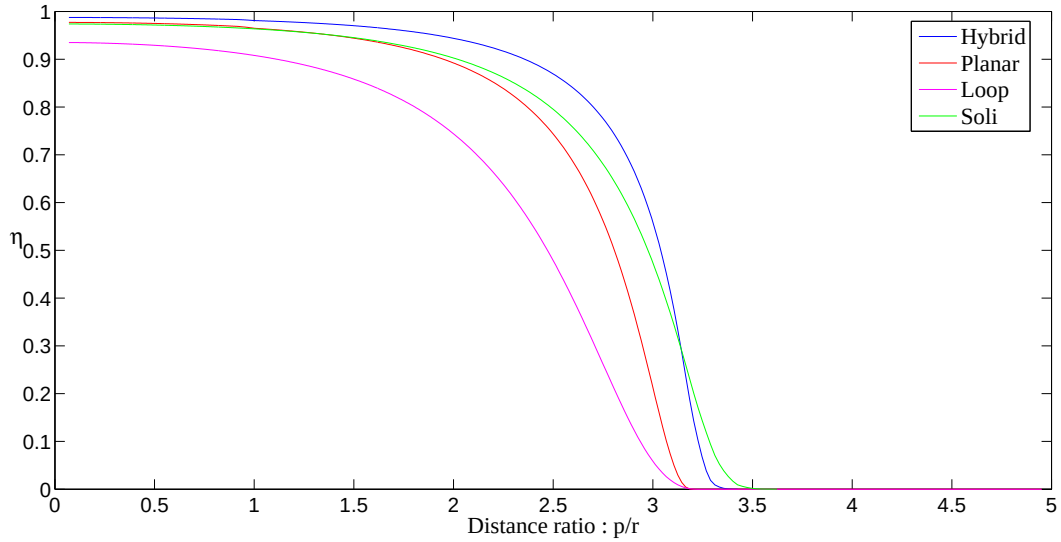

FIGURE 8.3: The efficiency as a function of the displacement between coil centres.

8.2.4 Discussion

Of the coil types discussed in this dissertation, the hybrid coil is the least affected by a displacement between the coil centres, until the displacement becomes larger than about three times the coil radius, at which point the solenoidal coil starts performing better than the hybrid coil. The planar coil initially performs better than the solenoidal coil, but after a displacement of

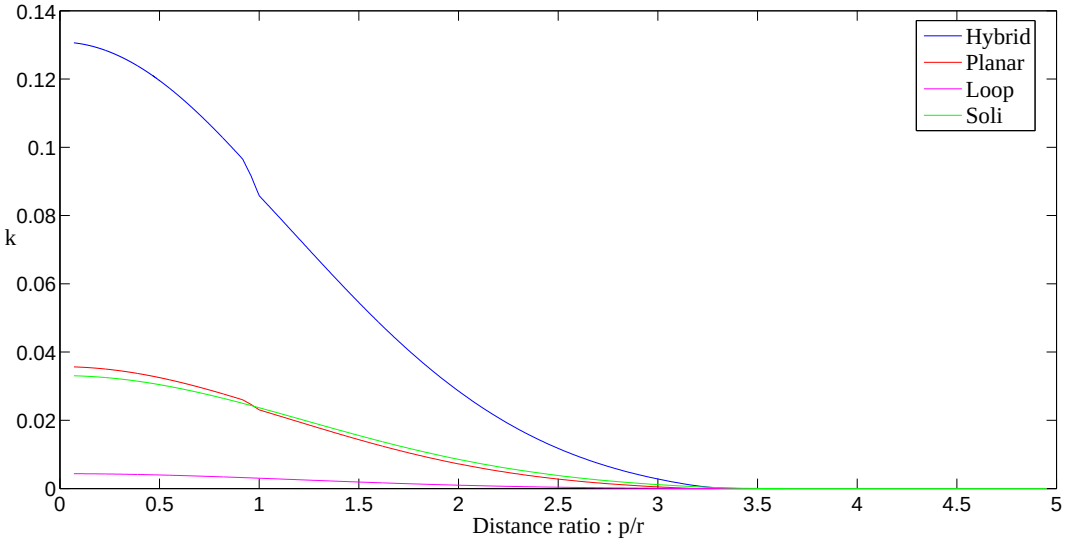

FIGURE 8.4: The coupling coefficient as a function of the displacement between coil centres.

about one coil radius the solenoidal coil's performance exceeds that of the planar coil. Between a displacement of three and three and a half coil radii, the efficiency dies away to zero for all coil types. This shows that the system is influenced to a much greater extent by a displacement between the coil centres than by a separation between the coils.

The coupling coefficients shows the effect of the displacement much clearer than the efficiencies does. A clear degradation in the coupling coefficients can be seen at a displacement of one coil radius. This is due to the fact that after a displacement of one coil radius, there are no more overlap of the various coil's uttermost turns, which has the largest radii and is responsible for the largest part of the mutual inductance between the coils. As with the efficiency plot, the coupling coefficient dies away to zero after a displacement of three to three and a half coil radii.

8.3 WIRE RADIUS

The wire radius plays an important role in the efficiency of a system. This section investigates the effect of the wire radius on both the efficiency of the system and the coupling coefficient between the coils. The effects are investigated only for single loops and for planar coils, because these two coil types demonstrate the effects of the wire radius adequately.

8.3.1 Theoretical background

The wire radius plays a role in several of the calculations to determine the efficiency of the system. The inductance of a single loop is influenced by the wire radius (Equation 5.7), as is the absorption resistance of the loop (Equation 5.16). Because these two parameters change with the wire radius, the centre frequency of the coil also change with the wire radius, as well as the figure-of-merit of the system and the system efficiency. The case of a planar coil is much more complicated than is the case for a single loop. The number of turns that can be fit inside a planar coil is determined by the wire radius. According to Zierhofer and Hochmair [12] the effect of adding more turns to a planar coil becomes negligible for turns smaller than $0.4r_{max}$ where r_{max} refers to the outermost turn of the coil. The number of turns that can be fit into a planar coil is then determined as:

$$N = \frac{0.4 \cdot r_{max}}{a}. \tag{8.5}$$

8.3.2 Algorithm

The algorithm used to investigate the effect of the wire radius on the efficiency of a single loop is shown in Algorithm 11. Algorithm 12 shows the algorithm used in the case of a planar coil. The mutual inductance between two single loops is not dependent on the wire radius (assuming that $a << R$) which means that it can be determined outside the loop which increases the wire radius, thereby saving processing time and -power. The mutual inductance as well as the self-inductance of planar coils are dependent on the number of turns, which changes as the wire radius change.

8.3.3 Simulation results

The effect of the wire radius on the efficiency of a single loop system is shown in Figure 8.5 while the effect on the coupling coefficient is shown in Figure 8.6. The effect on the efficiency and coupling coefficient for a planar coil system is shown in Figures 8.7 and 8.8, respectively.

8.3.4 Discussion

For single loops, the efficiency and the coupling coefficient increases with the wire radius. The reason for this is that the influence of the wire radius on the mutual coupling between the coils

Algorithm 11 An algorithm to investigate the influence of the wire radius on the efficiency.

determine M
for a = $small\_a$ to $large\_a$ **do**
  determine L
  for $frek$ = $start\_frek$ to $stop\_frek$ **do**
    determine loss rates
    determine efficiency
  end for
  determine optimal frequency
  henceforth, use optimal frequency
  determine loss rates
  determine efficiency
end for

Algorithm 12 An algorithm to investigate the influence of the wire radius on the efficiency for a planar coil.

determine M
for a = $small\_a$ to $large\_a$ **do**
  determine N
  if N == $N_{previous}$ **then**
    determine L
  else
    determine turn radii
    determine M
  end if
  for $frek$ = $start\_frek$ to $stop\_frek$ **do**
    determine loss rates
    determine efficiency
  end for
  determine optimal frequency
  henceforth, use optimal frequency
  determine loss rates
  determine efficiency
end for

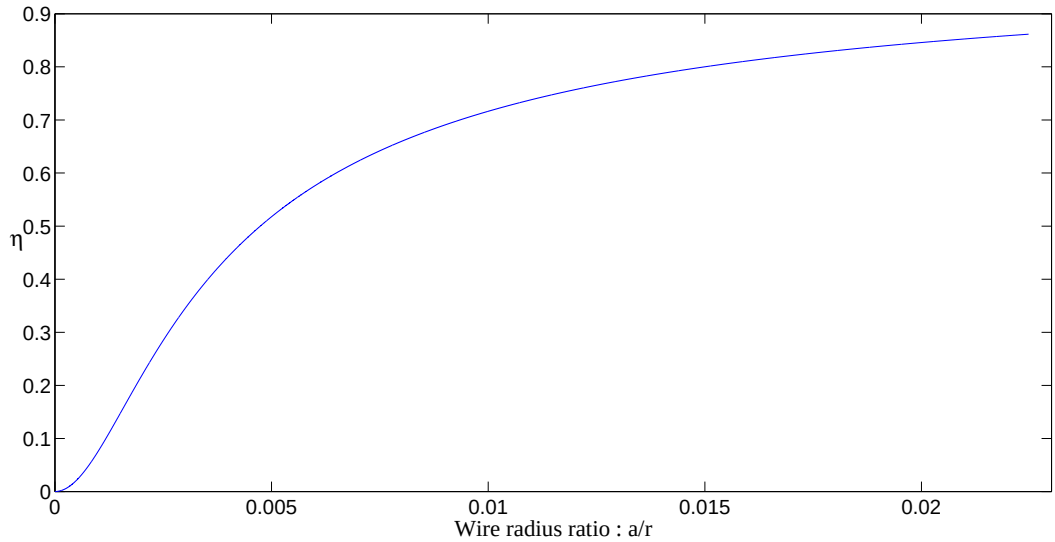

FIGURE 8.5: The efficiency of a single loop as a function of the wire radius.

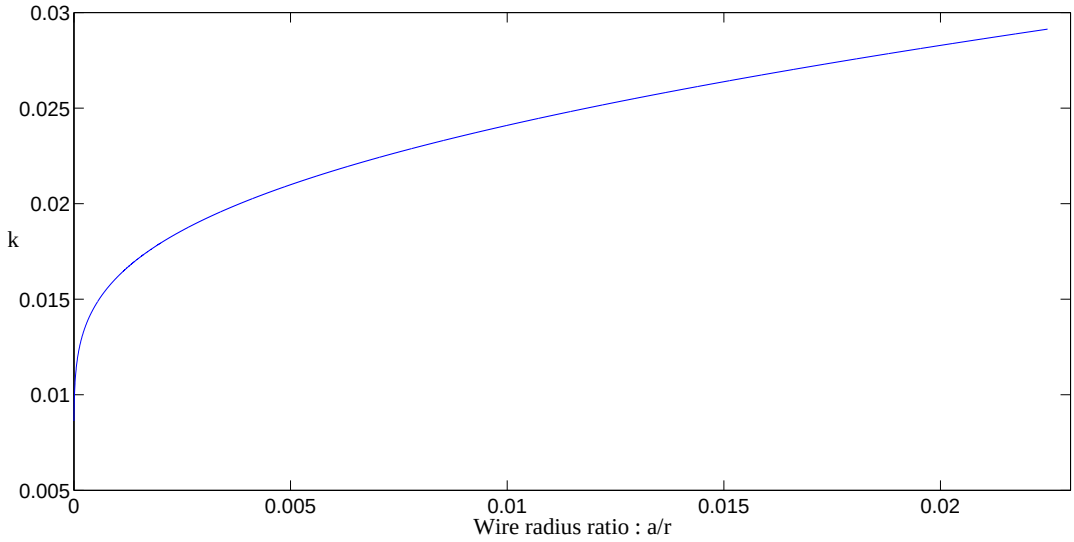

FIGURE 8.6: The coupling coefficient of a single loop as a function of wire radius.

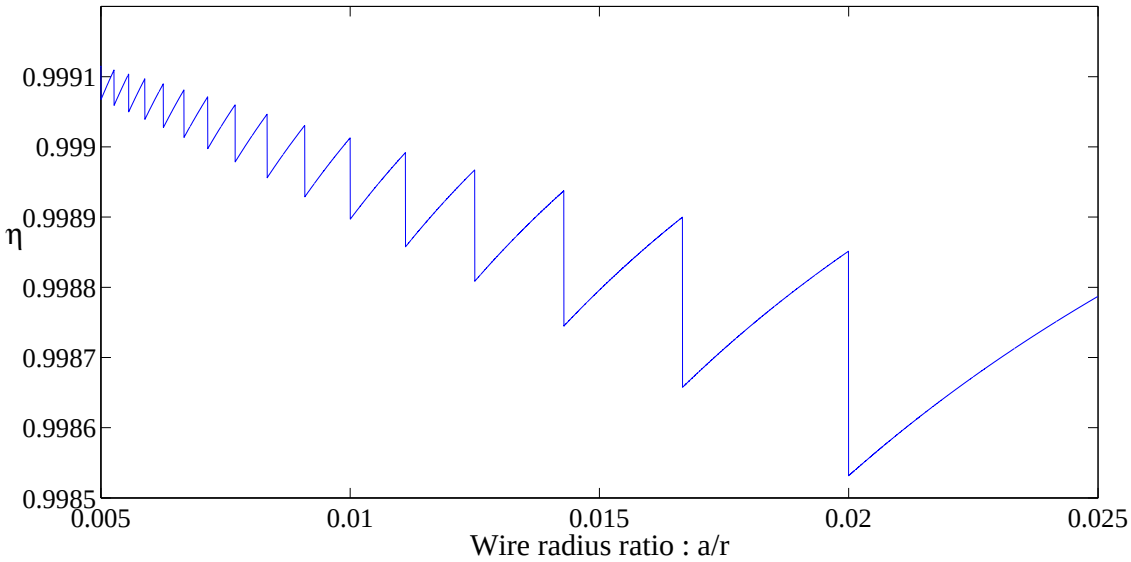

FIGURE 8.7: The efficiency of a planar coil as a function of the wire radius.

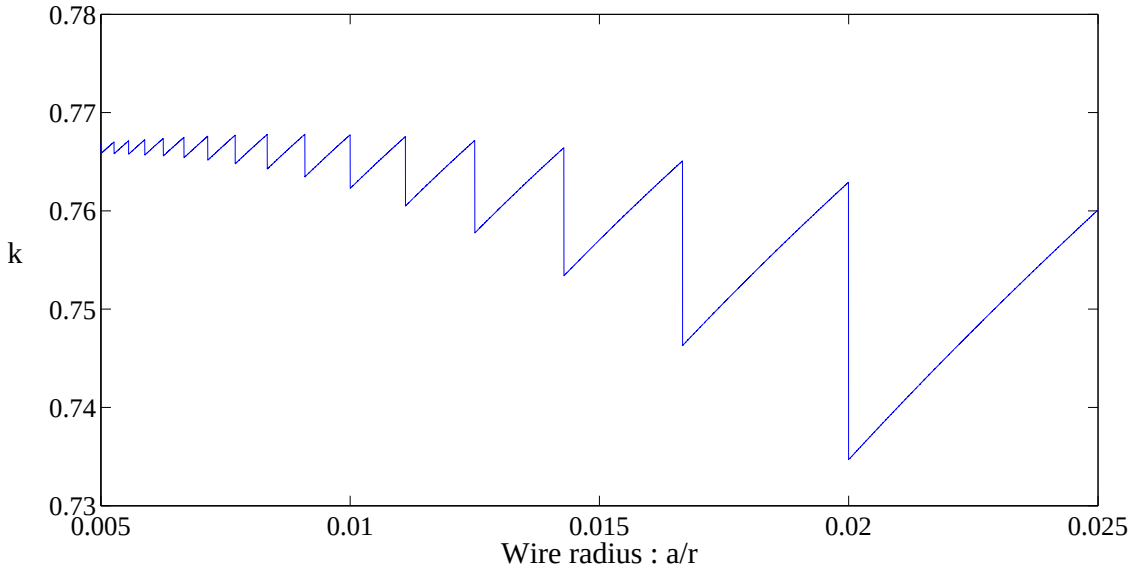

FIGURE 8.8: The coupling coefficient of a planar coil as a function of the wire radius.

is minimal, while the self-inductance of the coils decreases as the wire radius increase (see Equation 5.7). From Equation 2.1 it is clear that the coupling coefficient will increase as the self-inductance decrease.

In the case of planar coils the coupling coefficient and the efficiency decrease as the wire radius increase. The reason for the phenomenon is that the number of turns that can be fit within the coil area decreases as the wire radius increase. Both Figures 8.7 and 8.8 exhibits saw-tooth like behaviour. Each drop in efficiency or coupling coefficient correlates to a decreased number of turns that can be fit within the coil area. After each drop the efficiency and the coupling coefficient increases again as the wire radius increase. This shows the importance of optimally utilizing the inner area of the coil.

8.4 LARGER PRIMARY COIL

One way to increase the power transfer efficiency of the system without increasing the size of the receiver coil is to increase the size of the transmitter coil. Even though the transmitter coil is then larger than the receiver coil, the efficiency of the power transfer should increase.

8.4.1 Theoretical background

The influence of increasing the primary coil size is twofold. Both the coupling coefficient between the two coils and the loss rates of the primary coil are changed. The equations for the mutual inductance (Equation 5.18), the absorption resistance (Equation 5.16) and for the radiation resistance (Equation 5.15) still holds, though the values for the coil radii will not be equal as was the case before.

8.4.2 Algorithm

Algorithm 13 was written to investigate the effects of increasing the primary coil's radius. The algorithm scans over both increased primary coil radius and separation distance. The reason for this is that the effects of an increased primary coil radius is dependent on the separation distance.

Algorithm 13 An algorithm to investigate the effects of increasing the primary coil radius.

determine L_r
determine receiver loss rates
for r_t = $small$ to r_t = $large$ **do**
  for D = $small$ to D = $large$ **do**
    determine L_t
    determine M
    determine k
    determine transmitter loss rates
    determine η
  end for
end for

8.4.3 Simulation results

Figure 8.9 shows the coupling coefficient between the coils as a function of both the primary coil radius and the separation distance. Figure 8.10 shows the efficiency of the system, again as a function of the primary coil radius and the separation distance between the two coils. Figure 8.11 shows a normalized plot of the coupling coefficient and the efficiency of the system, both as functions of the primary coil radius.

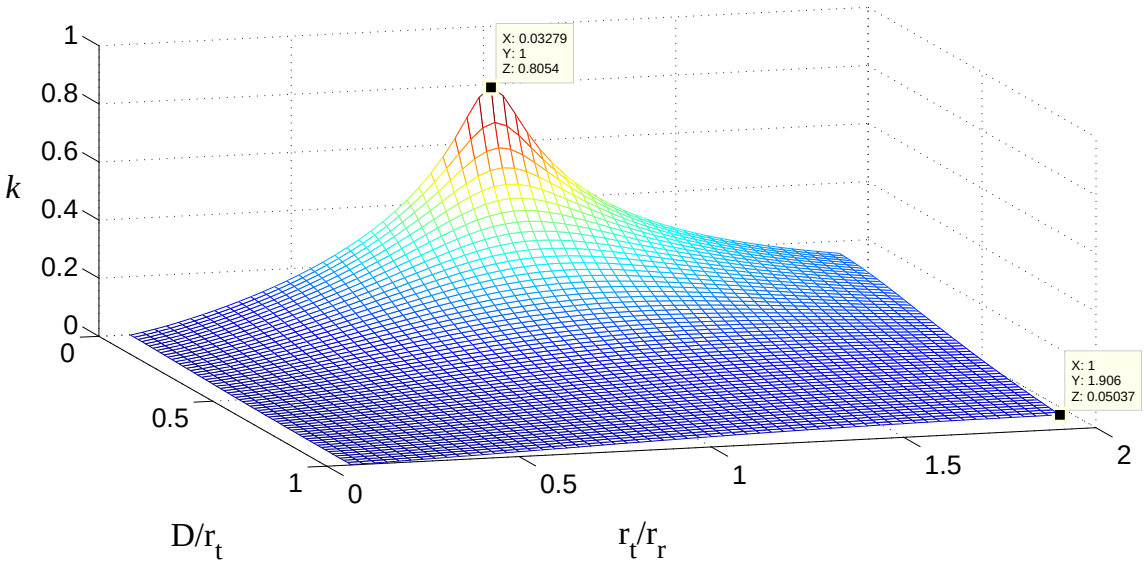

FIGURE 8.9: The coupling coefficient as a function of the primary coil radius and the separation distance.

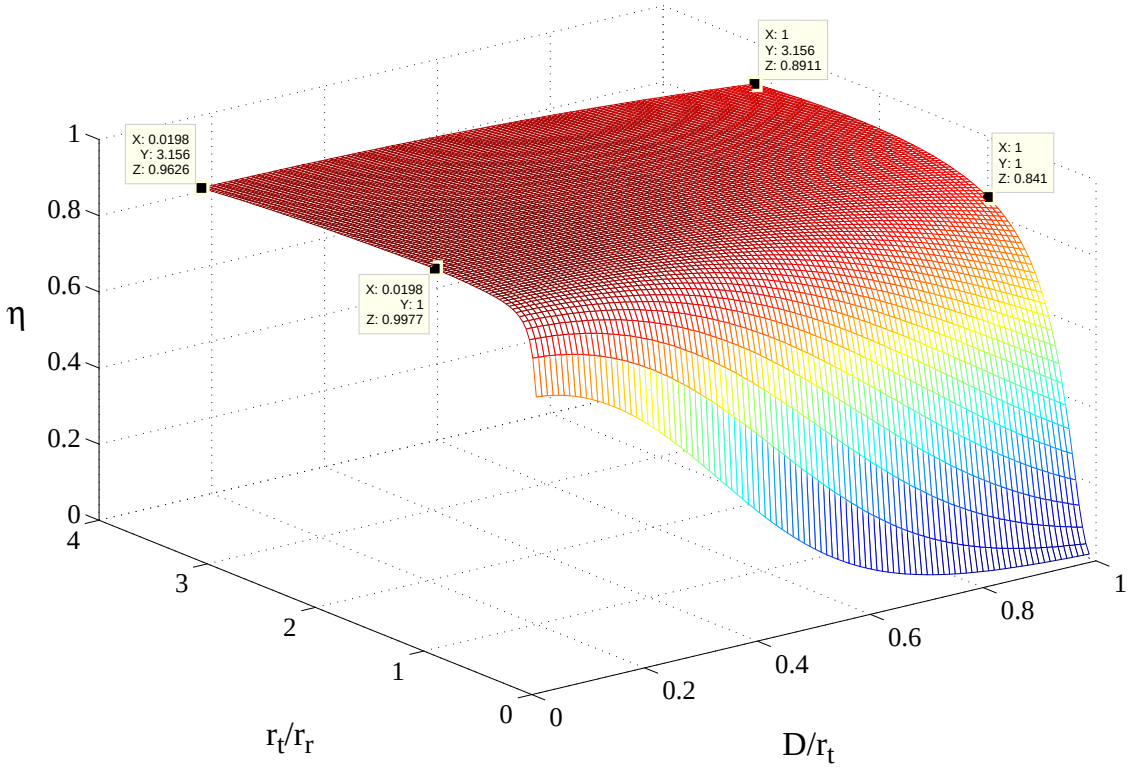

FIGURE 8.10: The efficiency as a function of the primary coil radius and the separation distance.

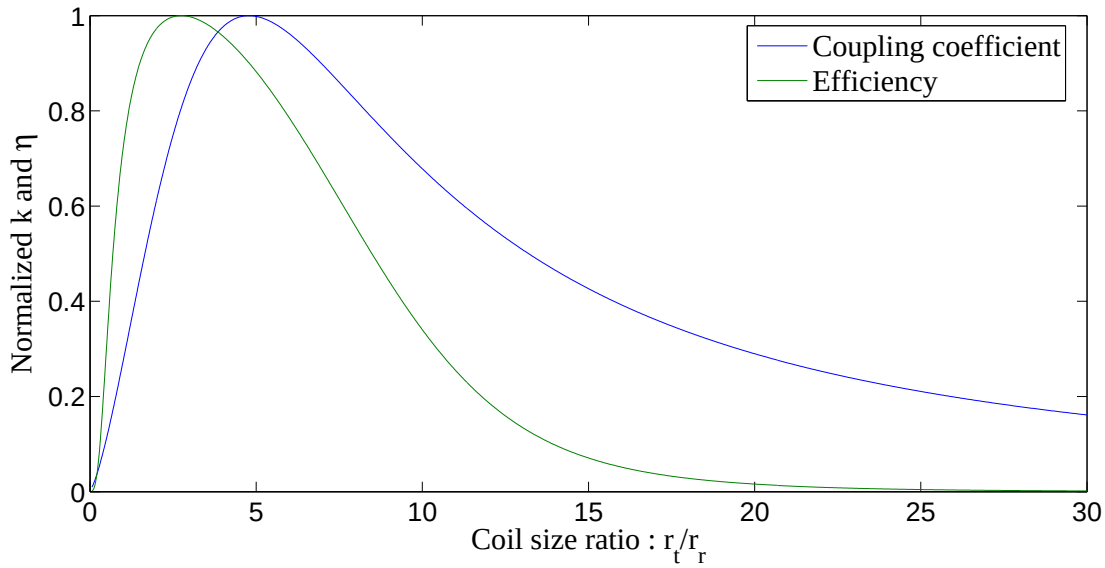

FIGURE 8.11: The normalized coupling coefficient and the efficiency as functions of the primary coil radius.

8.4.4 Discussion

Figure 8.9 shows that for small separation distances, the coupling coefficient of the system is highest when the two coils are exactly the same size. In this case an increase in transmitter coil radius does not improve the coupling coefficient once it becomes larger than the receiver coil. As the separation distance increase, the coupling coefficient starts increasing as the ratio between the transmitter coil radius and the receiver coil radius increases. In Figure 8.9 there is a distinct increase in coupling coefficient at $D/r_t = 1$ as the r_t/r_r relationship increase.

The efficiency of the system, shown in Figure 8.10, shows very similar behaviour to that of the coupling coefficient shown in Figure 8.9. For small separation distance, there is a small decrease in efficiency as the r_t/r_r relation exceeds unity. At larger separation distances, the efficiency increase as the primary coil radius increase. At a separation of one transmitter coil radius, the efficiency of the system is 5% higher for a transmitter coil radius of $3.1 \cdot r_r$ than for a transmitter coil radius of $1 \cdot r_r$. From Figure 8.10 it is clear that the efficiency of the system cannot be increased infinitely by increasing the primary coil radius.

Figure 8.11 is an normalized plot of the coupling coefficient and the efficiency of the system against the ratio between the transmitter and receiver coil radii. This figure shows that the efficiency and the coupling coefficient does not peak at the same coil radius ratio. Figure 8.11 was created for a separation distance of $D = 5 \cdot r_r$. The reason that the efficiency peaks at a smaller transmitter coil size is that it is dependent on the loss rates, which increase as the coil radius increase. The coupling coefficient is only dependent on the mutual inductance and on the self-inductances.

8.5 MIXED COIL TYPES

In this Section a system consisting of a single loop and a solenoidal coil is investigated. If the size for either the receiving coil or the transmitting coil is more stringent than for the other coil, the one coil can be a single loop while the other is one of the other coil types. In this way the efficiency of the system can be increased while keeping one of the two coils small.

8.5.1 Theoretical background

The parameters for each of coils is unchanged. The greatest influence of mixing coil types is that the mutual inductance, and hence the coupling coefficient, of the system will change.

The mutual inductance of the single loop and solenoidal coil system can be determined with Equation 8.6:

$$M = \sum_{j=1}^{N} M(r_{sl}, r_{sol}, D_j) \tag{8.6}$$

where r_{sl} is the radius of the single loop and r_{sol} the radius of the solenoidal coil. Care must also be taken to remember that the loss rates of the two coils now differs, unlike previous cases where the parameters for the transmitting and receiving coils were identical.

8.5.2 Algorithm

Algorithm 14 was written to investigate a system that uses two different coil types as transmitting coil and receiving coil. The algorithm determines the efficiency of the system over different separation distances. This was done in order to be able to compare the results of such a system with those of systems that uses only one type of coil, as investigated in Chapter 6.

Algorithm 14 An algorithm to investigate the efficiency of a system using two different coil types.

```
determine single loop inductance
determine solenoidal coil inductance
determine single loop loss rates
determine solenoidal coil loss rates
for D = small to D = large do
    determine M
    determine k
    determine η
end for
```

8.5.3 Simulation results

Figure 8.12 shows the results of a system that consists of a single loop and a solenoidal coil. The efficiencies (Chapter 6) of a single loop system and of a solenoidal coil system are also shown.

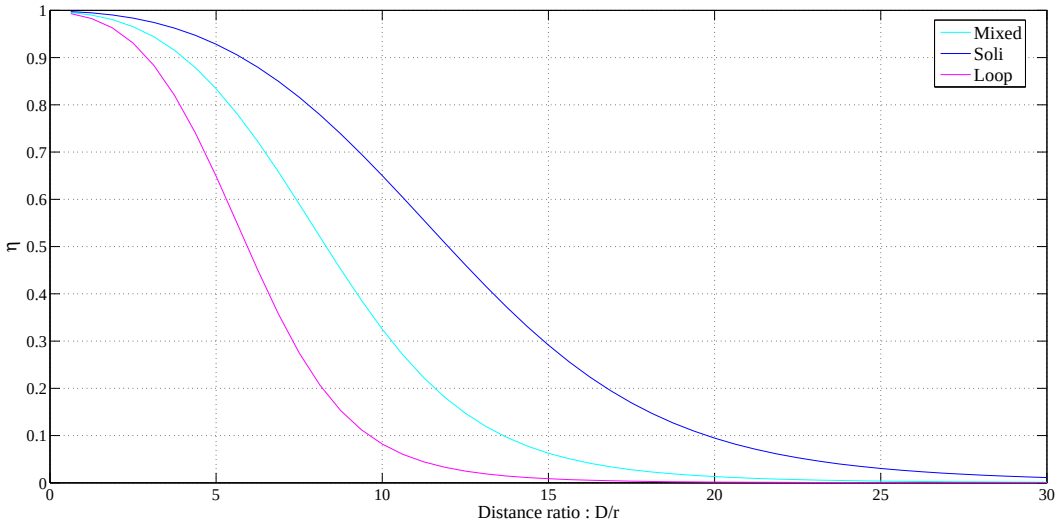

FIGURE 8.12: The efficiency of a system using mixed coil types.

8.5.4 Discussion

As expected, the mixed system outperforms the single loop system, while the solenoidal coil system outperforms the mixed coil system. This shows that it is possible to design a system with different coils, with design focus on reduced size for a specific coil while choosing another coil type for the other coil in order to increase efficiency.

CHAPTER NINE
CONCLUSION

THIS chapter gives a conclusion as to the work that was discussed in this dissertation. The validity of the hypotheses that was formulated in Chapter 1 is discussed and future work in this field is proposed.

9.1 RESEARCH SUMMARY

The problem of whether it is feasible to recharge WSN nodes with magnetic inductive power transfer was addressed by investigating various types of coils with special regard to their power transfer efficiency over distance. Coil types that were investigated are:

- single loops,
- solenoidal coils,
- planar coils,
- and hybrid coils.

The theoretical background for magnetically coupled, strongly resonant power transfer [2] [17] was adopted for use with solenoidal coils, planar coils and hybrid coils.

Algorithms was written to simulate the efficiency of each coil type, as well as to determine the influence of coil parameters such as frequency mismatching, coil misalignment and the wire radius.

A new coil type, the hybrid coil, was developed and mathematically modelled. It was shown to perform better than any of the other coil types. The different coil types were built

experimentally. The experimental results were compared to the theoretical results. The effect of parameter tolerances on the system efficiency was investigated.

9.2 RESULTS SUMMARY

The coils were investigated both theoretically and experimentally. The experimental self-inductances of the coils and the coupling coefficients of the coils are in good agreement with the theoretical results. The experimental efficiency of the coils is much smaller than the theoretical results. It was shown that frequency mismatching between the coils causes the efficiency of the system to drop, as seen in the experimental results.

The effect of displacement between the centres of the coils was investigated. It was shown that both the coupling coefficient and the efficiency of the system becomes smaller as the displacement is increased, and dies away when the displacement becomes larger than about three times the coil radius.

It was shown that the efficiency of the system is best when the area available to a coil is optimally utilized. A trade-off exists between the number of turns that can be used and the wire thickness. In the case of single loops the efficiency simply increases as the wire radius increase. In the case of planar coils, the number of turns is determined by the wire thickness. If the wire thickness is too large, very few turns can be fit into the planar coil, thereby decreasing the efficiency.

The effect of increasing the primary coil radius was investigated. It was shown that both the coupling coefficient and the efficiency of the coil can be enhanced in a limited way by increasing the transmitter radius. Once the transmitter radius becomes too large, the coupling coefficient and the efficiency drops again. This phenomenon suggests that, within the framework of this study, there is an absolute minimum receiver coil radius in order to achieve a required efficiency.

9.3 HYPOTHESIS EVALUATION

The hypothesis developed in Section 1.4.1 can now be evaluated in light of the experimental results. The hypothesis is:

> Magnetic inductive techniques can be used to recharge WSN nodes over a medium sized office by using inductive coils that are effective in terms of power transfer efficiency, cost and size comparable to a WSN node.

As neither the theoretical results nor the experimental results, even when using the new hybrid coil, could achieve the efficiency needed over the distance needed as described in Section 4.4, the hypothesis is rejected. In it s place a new hypotheses is formulated:

> Magnetic inductive techniques cannot be used to recharge WSN nodes over a medium sized office by using inductive coils in a way that is effective, as per our definition, in terms of power transfer efficiency, cost and size comparable to a WSN.

As the theoretical results and the experimental results has shown that the efficiency over the required distance is lower than the specified efficiency, this hypothesis will be accepted.

9.4 RESEARCH CONTRIBUTION

This research contributed to the body of knowledge in that:

- it was shown that magnetic inductive techniques are not a feasible solution, as we defined it, to recharge WSN nodes,
- the magnetically coupled, strongly resonant power transfer method of Karalis *et al* was adapted for use with solenoidal, planar and hybrid coils,
- a new coil type, the hybrid coil, was developed and shown to be more efficient than single loops, solenoidal coils and planar coils,
- the effects of parameter tolerances on the efficiency of a system were investigated,
- and algorithms were created to determine the coil parameters of each coil type.

9.5 FUTURE WORK

Even though magnetic inductive power transfer techniques are not a feasible solution for WSNs, there are other applications in which it can be used:

- Wireless recharging of small devices such as PDAs and mobile phones. Except for the advantage of being very convenient, the wireless recharging of small devices also serves to isolate them from fluctuations in the power grid.

- Wireless powering of devices such as wireless earphones and gamestation controllers. The advantages of powering these devices wirelessly are that it decreases the weight of the devices in the case of previously battery powered devices, and it allows more freedom of movement in cases where wires were used to power the devices.

Other work that is of interest is:

- to increase the power transfer efficiency with techniques such as Litz wire,
- to investigate the possibility of using printed planar coils instead of wire coils, with special regard to an investigation as to which is more efficient: a large number of thin turns, or one very thick loop,
- a thorough investigation of the effects of the proximity of a magnetic inductive power transfer system on devices containing magnetic elements such as CRT screens,
- an in-depth study as to the effect of high frequency magnetic inductive power transfer systems on human health and safety,
- and to confirm the theoretical efficiency of the hybrid coil using low tolerance manufacturing techniques.

9.6 FINAL CONCLUSION

While magnetic inductive power transfer is not likely to be applied to WSNs in the near future, it is a field with great potential. In a world where environmental concerns such as the toxic elements contained in batteries are a very real problem, small-range magnetic inductive power transfer systems may provide a convenient way to recharge batteries, making short battery life less of a problem than it currently is. This will allow smaller, less expensive and environmentally safer batteries to be used in some applications. In some cases batteries may even be substituted with supercapacitors, which has a much greater life-time than batteries.

Energy efficiency is a very important consideration in any design. The hybrid coil introduced in this study may provide a way of increasing the efficiency of a magnetic inductive power transfer system, thereby saving both energy and money.

In this Chapter the work done in this dissertation is concluded. The original hypothesis of Section 1.4.1 was found to be false, and a new hypothesis was formulated in view of the results

obtained in this dissertation. Future work is proposed and possible applications for magnetic inductive power transfer systems as described in this dissertation is presented.

REFERENCES

[1] C. M. Zierhofer and E. S. Hochmair, "High-efficiency coupling-insensitive transcutaneous power and data transmission via an inductive link," *IEEE Transactions on Biomedical Engineering*, vol. 37, no. 7, pp. 716–722, 1990.

[2] A. Kurs, A. Karalis, R. Moffatt, J. D. Joannopoulos, P. Fisher, and M. Soljacic, "Wireless power transfer via strongly coupled magnetic resonances," *Science*, vol. 317, no. 5834, pp. 83–86, 2007.

[3] J. Pan, B. Xue, and Y. Inoue, "A self-powered sensor module using vibration-based energy generation for ubiquitous systems," *ASICON 2005: 2005 6th International Conference on ASIC, Proceedings*, vol. 1, pp. 443–446, 2005.

[4] M. Stordeur and I. Stark, "Low power thermoelectric generator - self-sufficient energy supply for micro systems," *International Conference on Thermoelectrics*, pp. 575–577, 1997.

[5] J. A. Paradiso and T. Starner, "Energy scavenging for mobile and wireless electronics," *IEEE Pervasive Computing*, vol. 4, no. 1, pp. 18–27, 2005.

[6] H. Körber, H. Wattar, and G. Scholl, "Modular wireless real-time sensor/actuator network for factory automation applications," *IEEE Transactions on Industrial Informatics*, vol. 3, no. 2, pp. 111–118, 2007.

[7] S. R. Anton and H. A. Sodano, "A review of power harvesting using piezoelectric materials (2003-2006)," *Smart Materials and Structures*, vol. 16, no. 3, 2007.

[8] R. Morais, M. A. Fernandes, S. G. Matos, C. Serodio, P. J. S. G. Ferreira, and M. J. C. S. Reis, "A zigbee multi-powered wireless acquisition device for remote sensing applications in precision viticulture," *Computers and Electronics in Agriculture*, vol. 62, no. 2, pp. 94–106, 2008.

[9] N. N. Donaldson de and T. A. Perkins, "Analysis of resonant coupled coils in the design of radio frequency transcutaneous links," *Medical and Biological Engineering and Computing*, vol. 21, pp. 612–627, 1983.

[10] D. Galbraith, M. Soma, and R. L. White, "Wide-band efficient inductive transdermal power and data link with coupling insensitive gain." *IEEE Transactions on Biomedical Engineering*, vol. BME-34, no. 4, pp. 265–275, 1987.

[11] J. Schuder, H. Stephenson, and J. Townsend, "High-level electromagnetic energy transfer through a closed chest wall," *IRE International Convention Record*, vol. 9, pp. 119–126, 1961.

[12] C. M. Zierhofer and E. S. Hochmair, "Geometric approach for coupling enhancement of magnetically coupled coils," *IEEE Transactions on Biomedical Engineering*, vol. 43, no. 7, pp. 708–714, 1996.

[13] H. Sakamoto, K. Harada, S. Washimiya, K. Takehara, Y. Matsuo, and F. Nakao, "Large air-gap coupler for inductive charger," *IEEE Transactions on Magnetics*, vol. 35, no. 5 PART 2, pp. 3526–3528, 1999.

[14] Y. Matsuda, H. Sakamoto, H. Shibuya, and S. Murata, "A non-contact energy transferring system for an electric vehicle-charging system based on recycled products," *Journal of Applied Physics*, vol. 99, 2006.

[15] J. Wu, V. Quinn, and G. H. Bernstein, "Powering efficiency of inductive links with inlaid electroplated microcoils," *Journal of Micromechanics and Microengineering*, vol. 14, no. 4, pp. 576–586, 2004.

[16] C. R. Neagu, H. V. Jansen, A. Smith, J. G. E. Gardeniers, and M. C. Elwenspoek, "Characterization of a planar microcoil for implantable microsystems," *Sensors and Actuators, A: Physical*, vol. 62, no. 1-3, pp. 599–611, 1997.

[17] A. Karalis, J. D. Joannopoulos, and M. Soljacic, "Efficient wireless non-radiative mid-range energy transfer," *Annals of Physics*, vol. 323, no. 1, pp. 34–48, 2008.

[18] T. Aoki, B. Dayan, E. Wilcut, W. P. Bowen, A. S. Parkins, T. J. Kippenberg, K. J. Vahala, and H. J. Kimble, "Observation of strong coupling between one atom and a monolithic microresonator," *Nature*, vol. 443, no. 7112, pp. 671–674, 2006, cited By (since 1996): 40.

[19] J. A. Hagerty, F. B. Helmbrecht, W. H. McCalpin, R. Zane, and Z. B. Popovi, "Recycling ambient microwave energy with broad-band rectenna arrays," *IEEE Transactions on Microwave Theory and Techniques*, vol. 52, no. 3, pp. 1014–1024, 2004.

[20] M. Takamiya, T. Sekitani, Y. Miyamoto, Y. Noguchi, H. Kawaguchi, T. Someya, and T. Sakurai, "Design solutions for a multi-object wireless power transmission sheet based on plastic switches," 2007.

[21] M. Takamiya, T. Sekitani, Y. Kato, H. Kawaguchi, T. Someya, and T. Sakurai, "An organic fet sram with back gate to increase static noise margin and its application to braille sheet display," *IEEE Journal of Solid-State Circuits*, vol. 42, no. 1, pp. 93–99, 2007.

[22] H. L. Cheng, Y. C. Hsieh, and C. H. Lin, "A novel single-stage high-power-factor ac/dc converter featuring high circuit efficiency," 2009.

[23] Z. N. Low, R. A. Chinga, R. Tseng, and J. Lin, "Design and test of a high-power high-efficiency loosely coupled planar wireless power transfer system," *IEEE Transactions on Industrial Electronics*, vol. 56, no. 5, pp. 1801–1812, 2009.

[24] A. Kangarlu and P. . L. Robitaille, “Biological effects and health implications in magnetic resonance imaging,” *Concepts in Magnetic Resonance*, vol. 12, no. 5, pp. 321–359, 2000.

[25] *MICAz Datasheet*, Crossbow Technology, Inc., 4145 North First Street San Jose, California 95134-2109, April 2007, 6020-0060-04 Rev A.

[26] A. Ahlbom, U. Bergqvist, J. H. Bernhardt, J. P. Cesarini, L. A. Court, M. Grandolfo, M. Hietanen, A. F. McKinlay, M. H. Repacholi, D. H. Sliney, J. A. J. Stolwijk, M. L. Swicord, L. D. Szabo, M. Taki, T. S. Tenforde, H. P. Jammet, and R. Matthes, “Guidelines for limiting exposure to time-varying electric, magnetic, and electromagnetic fields (up to 300 ghz),” *Health Physics*, vol. 74, no. 4, pp. 494–521, 1998.

[27] H. Haus, *Waves and Fields in Optoelectronics*. Prentice-Hall, New Jersey, 1984.

[28] H. A. Haus and W. Huang, “Coupled-mode theory,” *Proceedings of the IEEE*, vol. 79, no. 10, pp. 1505–1518, 1991.

[29] B. Guru and H. Hiziroglu, *Electromagnetic Field Theory Fundamentals, 2nd Edition*. Cambridge University Press, 2004.

[30] A. Karalis. (2009, September) Personal communication - student enquiry regarding ”efficient wireless non-radiative mid-range,energy transfer”. aristos@mit.edu.

[31] J. Van Deun and R. Cools, “Integrating products of bessel functions with an additional exponential or rational factor,” *Computer Physics Communications*, vol. 178, no. 8, pp. 578–590, 2008.